

Resolving temperature **limitation** on spring productivity in an evergreen conifer forest using a model-data fusion framework

Stephanie G. Stettz¹, Nicholas C. Parazoo², A. Anthony Bloom², Peter D. Blanken³, David R. Bowling⁴, Sean P. Burns^{3,5}, Cédric **Bacour**⁶, Fabienne **Maignan**⁷, Brett Raczka⁵, Alexander J. **Norton**², Ian **Baker**⁸, Mathew **Williams**^{9,10}, Mingjie **Shi**¹¹, Yongguang **Zhang**¹², Bo Qiu¹²

¹Department of Earth System Science, University of California Irvine, Irvine, California, USA

²Jet Propulsion Laboratory, California Institute of Technology, Pasadena, California, USA

³Department of Geography, University of Colorado Boulder, Boulder, Colorado, USA

⁴[School of Biological Sciences, University of Utah, Salt Lake City, Utah, USA](#)

⁵[National Center for Atmospheric Research, Boulder, Colorado, USA](#)

⁶NOVELTIS, 153 rue du Lac, 31670 Labège, France

⁷Laboratoire des Sciences du Climat et de l'Environnement, LSCE/IPSL, CEA-CNRS-UVSQ, Université Paris-Saclay, Gif-sur-Yvette, France

⁸Cooperative Institute for Research in the Atmosphere, Colorado State University, Fort Collins, Colorado, USA

⁹School of GeoSciences and National Centre for Earth Observation, University of Edinburgh, Edinburgh, UK

¹⁰National Centre for Earth Observation, Edinburgh EH9 3FF, Edinburgh, UK

¹¹[Pacific Northwest National Laboratory, 902 Battelle Blvd, Richland, WA 99354](#)

¹²International Institute for Earth System Sciences, Nanjing University, Nanjing, Jiangsu Province, China

*Correspondence to: Stephanie Stettz (sstettz@uci.edu)

Abstract

[The flow of carbon through terrestrial ecosystems and the response to climate is a critical but highly uncertain process in the global carbon cycle](#). However, with a rapidly expanding array of in situ and satellite data, there is an opportunity to improve our mechanistic understanding of the carbon (C) cycle's response to land use and climate change. Uncertainty in temperature **limitation** on productivity poses a significant challenge to predicting the response of ecosystem carbon fluxes to a changing climate. Here we diagnose and quantitatively resolve environmental limitations on growing season onset of gross primary production (GPP) using nearly two decades of meteorological and C flux data (2000-2018) at a subalpine evergreen forest in Colorado, USA. We implement the CARDAMOM model-data fusion network to resolve the temperature sensitivity of spring GPP. To capture a GPP temperature **limitation**—a critical component of integrated sensitivity of GPP to temperature—we introduced a cold temperature scaling function in CARDAMOM to regulate photosynthetic productivity. We found that GPP was gradually inhibited at **temperature** below 6.0 °C (± 2.6 °C) and completely inhibited below -7.1 °C (± 1.1 °C). The addition of this scaling factor improved the model's ability to replicate spring GPP at interannual and decadal time scales ($r = 0.88$), relative to the nominal CARDAMOM configuration ($r = 0.47$), and improved spring GPP model predictability outside of the data assimilation training period ($r = 0.88$). While cold temperature limitation has an important influence on spring GPP, it does not have a significant impact on integrated growing season GPP, revealing that other environmental controls, such as [precipitation](#), play a more important role in annual productivity.

41 This study highlights growing season onset temperature as a key limiting factor for spring growth in [winter-dormant](#)
42 evergreen forests, which is critical in understanding future responses to climate change.

43 1. Introduction

44 Northern hemisphere evergreen forests contribute significantly to terrestrial carbon (C) storage and exchange
45 (Beer et al., 2010; Thurner et al., 2014). High-[latitude and high-elevation](#) evergreen forests show increasing gross
46 primary productivity (GPP) with increasing temperature driven in large part by earlier growing seasons (Myneni et
47 al., 1997; Randerson et al., 1999; Forkel et al., 2016; Winchell et al., 2016, Lin et al., 2017). However, the response
48 of gross and net C fluxes to warming remains uncertain, especially in subalpine temperate forests, which can
49 experience freezing temperature while still absorbing large amounts of sunlight; both these factors ultimately
50 influence the timing and magnitude of GPP (Bowling et al., 2018). In particular, warmer springs can also lead to
51 earlier snowmelt, which can reduce spring C uptake through increased surface exposure to colder ablation-period air
52 temperatures (Winchell et al., 2016), and can reduce summer C uptake via drought (Hu [et al., 2010](#)). Many
53 subalpine forests in western North America are also highly water limited, with warming and earlier snow melt
54 creating accumulated water deficits, increased drought stress, and growing season C uptake losses (Wolf et al.,
55 2016; Sippel et al., 2017; Buermann et al., 2018, Goulden and Bales, 2019); these factors ultimately make subalpine
56 forest ecosystems sensitive to the direct and indirect effects of climate change and other disturbances, including the
57 effects of droughts, fires and insect infestations ([Keenan et al., 2014](#); [Frank et al., 2014](#); Knowles et al., 2015). The
58 uncertainty in the temperature sensitivity of springtime GPP, increasing vulnerability to [disturbance](#), and GPP
59 modeling challenges (Anav et al., 2015) create urgency to improve our ability to observe and model these
60 ecosystems to understand how C exchange will be altered in a warming climate.

61 Fortunately, availability of long term ecosystem observations is improving. The expansion of international
62 flux tower networks over the last three decades (e.g. AmeriFlux, FLUXNET, ChinaFLUX, ICOS) has greatly
63 improved C flux sampling across global ecosystems at 1 km scale ([Baldocchi 2008](#); [Baldocchi et al., 2018](#)), and the
64 number of spaceborne sensors continues to grow, allowing global estimation of gross primary production (GPP) and
65 net ecosystem C exchange (NEE) over the last decade (e.g. Stavros et al., 2017; Sun et al., 2017; Schimel et al.,
66 2019). While uncertainties in estimating C fluxes from in situ and satellite data [remain](#) a challenge, the expanding
67 observational record offers a great opportunity to study the temperature sensitivity of subalpine forests at multiple
68 temporal scales.

69 The range of modeling tools available to quantify and study major C pools under ever growing
70 observational constraints is also increasing. Process-based models, in general terms, use explicit mathematical
71 relationships to mechanistically describe bio-physical processes ([Korzukhin et al., 2011](#); [Huxman et al., 2003](#);
72 [Keenan et al., 2012](#)). In contrast, model-data fusion (MDF) is a relatively new tool that alters model parameters [to](#)
73 [statistically reduce mismatches between observations and model predictions](#) (Raupach et al., 2005; Wang et al.,
74 2009; Keenan et al., 2012). MDF methods can be used to statistically represent the terrestrial C balance by
75 generating optimized state and process variable parameterizations, with uncertainties, which best match the signal
76 and noise in observations (Bloom et al., 2020).

Deleted: 1996

78 Models of varying complexity and assimilation capabilities have been used to study how C exchange varies
79 with temperature in subalpine evergreen ecosystems (e.g., Moore et al., 2008; Scott-Denton et al., 2013; Knowles et
80 al., 2018). Moore et al. (2008) used a simplified ecosystem function model and assimilated C flux data from the
81 Niwot Ridge (US-NR1) subalpine evergreen forest AmeriFlux tower in Colorado to show the importance of accurate
82 meteorological forcing for parameter optimization and the usefulness of assimilating C flux data for determining
83 connections between the C and water cycles. Scott-Denton et al. (2013) integrated meteorological and flux data
84 from 1999-2008 from the same site with an ensemble of more sophisticated Earth System Models (ESM) and
85 showed higher rates of C uptake by the end of the 21st century associated with warming and lengthening growing
86 seasons, and driven by greater increases of spring GPP relative to late season respiration.

87 Interestingly, model and empirical studies of the C flux response to climate at US-NR1 focus on the 2000-
88 2011 period, which saw increasing summer drought coupled with sustained declines in spring temperature and GPP.
89 US-NR1 has since experienced a gradual recovery of spring GPP with increased spring warming throughout 2011-
90 2018 (Fig. 1), which begs the question: what is the temperature sensitivity of spring GPP over multiple decades of
91 spring cooling and warming at US-NR1, and how well can data-constrained models reproduce long term variability?
92 To answer this question, we combine a mechanistic ecosystem C model (Data Assimilation Linked Ecosystem
93 Carbon, or DALEC2; Williams et al., 2005; Bloom et al., 2016) with the CARbon DAta-MODEl framEwork
94 (CARDAMOM; Bloom and Williams, 2015; Bloom et al., 2020) driven by observed meteorological forcing and
95 constrained against eddy covariance fluxes at US-NR1, to investigate the temperature sensitivity of this subalpine
96 evergreen forest at seasonal and interannual timescales. We introduce a new cold temperature limitation function,
97 trained on observed temperature, for more realistic simulation of spring GPP onset. The use of high quality and long
98 term (2000-2018) meteorology and partitioned GPP data at US-NR1 to drive and constrain the model enables robust
99 statistical analysis of interannual variability (IAV), and assessment of “model predictability” through training and
100 validation against subsets of data. We also leverage a recent model intercomparison study (Parazoo et al., 2020),
101 driven by site level meteorological data at US-NR1, to provide a model benchmark assessment, and extract any
102 common environmental controls on modeled GPP. Finally, we examine whether using a decade of flux tower-
103 derived GPP observations to train the model is sufficient to match and predict seasonal to annual patterns in GPP.
104 Given the complexity of carbon-water cycle interactions during the growing (summer) season in this highly water
105 limited ecosystem, and the relatively weak correlation between tower-derived spring and summer GPP ($r = -0.31$, p
106 $= 0.20$), we focus on spring GPP-temperature interactions, with the aim to resolve just one piece of the larger,
107 complex problem of understanding changes in C uptake in a subalpine evergreen ecosystem.

108 2. Materials & Methods

109 2.1. Study Site: Niwot Ridge, CO., USA

110 Our study focuses on an AmeriFlux (<https://ameriflux.lbl.gov/>) core site in Niwot Ridge, Colorado, USA
111 (US-NR1, 40°1'58''N; 105°32'47'' W), where a tower-based eddy covariance system has been used to continuously
112 monitor the net ecosystem exchange (NEE) of carbon dioxide over a subalpine forest since November 1998. The 26

Deleted: ure

Deleted: da

Deleted: l

Deleted: are

Deleted: sufficiently robust

Deleted: measuring

119 m tall tower is located in a high elevation (3050 m) subalpine site in the Rocky Mountains of Colorado (Monson et
120 al., 2002). Located in an evergreen needleleaf (ENF) ecosystem, the dominant tree species include lodgepole pine
121 (*Pinus contorta*), subalpine fir (*Abies lasiocarpa*), and Engelmann spruce (*Picea engelmannii*) (Turnipseed et al.,
122 2002; Turnipseed et al., 2004). Average annual precipitation is 800 mm, with a majority of precipitation falling in
123 the winter as snow (Greenland, 1989; Knowles et al., 2015), which creates a persistent winter snowpack from
124 November through early June (Bowling et al., 2018).

125 2.2. Observations

126 NEE measurements are screened for calm conditions using the standard u_{star} filtering, gap-filled, and
127 partitioned into GPP and ecosystem respiration based on the relationship between nighttime NEE
128 (photosynthetically active radiation, PAR < 50 $\mu\text{mol m}^{-2} \text{s}^{-1}$) and air temperature (Reichstein et al., 2005; Wutzler et
129 al., 2018). Monthly averages of GPP based on nighttime partitioning show similar seasonal structure to results found
130 using an alternative daytime partitioning algorithm (Lasslop et al., 2009), so only nighttime partitioned GPP data are
131 reported here. All GPP estimates are processed as half hourly means, then averaged monthly. Details on the flux
132 measurements, data processing and quality control are provided in Burns et al. (2015).

133 2.3. The CARDAMOM Model-Data Fusion System

134 The CARbon DAta-MODEl FramEwork (CARDAMOM; Bloom et al., 2016; Yin et al., 2020; Exbrayat et
135 al., 2018; Smallman et al., 2017; Quetin et al., 2020; López-Blanco et al., 2019; Famiglietti et al., 2021; Bloom et
136 al., 2020; amongst others) uses carbon cycle and meteorological observations to constrain carbon fluxes, states and
137 process controls represented in the DALEC2 model of terrestrial C cycling (Williams et al., 2005; Bloom and
138 Williams, 2015). Specifically, CARDAMOM uses a Bayesian model-data fusion approach to optimize DALEC2
139 time-invariant parameters (such as leaf traits, allocation and turnover times) and the “initial” C and H₂O conditions
140 (namely biomass, soil and water states at the start of the model simulation period).

141 The DALEC model (Williams et al., 2005; Rowland et al., 2014; Fox et al., 2009; Richardson et al., 2010;
142 Famiglietti et al., 2021; Bloom & Williams, 2015; amongst others) is a box model of C pools connected via fluxes
143 that has been used to evaluate terrestrial carbon cycle dynamics across a range of ecosystems and spatial scales. In
144 all site, regional, and global applications, DALEC parameters are subject to very broad, but physically realistic, prior
145 distributions, and independently estimated and constrained by available observations at each grid point. Here we use
146 DALEC version 2 (DALEC2; Yin et al., 2020; Quetin et al., 2020; Bloom et al., 2020); gross and net carbon fluxes
147 are determined as a function of 33 parameters, including 26 time-invariant parameters relating to allocation, turnover
148 times, plant traits, respiration climate sensitivities, water-use efficiency and GPP sensitivity to soil moisture, and 7
149 parameters describing the initial conditions of live biomass pools (live biomass C, dead organic C and plant-
150 available H₂O). Within DALEC2, GPP estimates are generated in the aggregated canopy model (ACM, Williams et
151 al., 1997); the ACM is derived from simple functional relationships with environmental and plant structural and
152 biochemical information (Williams et al., 1997), that are produced from a sensitivity analysis of GPP estimates from

Deleted: 10

Deleted: o

Deleted: 7

Deleted: 0

Deleted: 0

Deleted: which comprise

Deleted: of

Deleted: e

161 the more comprehensive SPA land surface model scheme (Williams et al., 1996, Williams et al., 2001). ACM GPP
 162 estimates are contingent on plant structural and biochemical variables (including LAI, foliar nitrogen and nitrogen-
 163 use efficiency) and meteorological forcing (total daily irradiance, maximum and minimum daily air temperature, day
 164 length, atmospheric CO₂ concentration). In DALEC2, water limitation on ACM is prescribed as a linear response to
 165 soil water deficit (Bloom et al., 2020). For more details on the model-data fusion methodology and CARDAMOM
 166 ensembles, we refer the reader to Appendix A. For a comprehensive overview of the DALEC2 model, we refer the
 167 reader to Bloom et al. (2020) and references therein.

Deleted: s

Deleted: ,

168 2.4. Experiment Design

169 In order to develop model experiments that could reliably evaluate temperature-GPP interactions, we first
 170 examine the observed environmental controls on tower-derived GPP. We focus on GPP during spring, defined here
 171 as the period from March-May, which encompasses the climatological onset of GPP and transition from dormant
 172 winter conditions to peak summer conditions (Fig. 1a). Mean spring GPP exhibits large interannual variability (IAV)
 173 with both a small decreasing trend from 2000-2010 ($-0.02 \text{ g C m}^{-2} \text{ day}^{-1} \text{ per year}$) and increasing trend from 2010-
 174 2018 ($0.04 \text{ g C m}^{-2} \text{ day}^{-1} \text{ per year}$) (Fig. 1b). Comparison to tower observed temperature data (Fig. 1b and Fig. 2)
 175 shows that spring GPP is positively correlated to mean spring air temperature (Pearson's linear $r = 0.89$, $p =$
 176 0.000004) and summer (June-September) air temperature ($r = 0.10$, $p = 0.70$, Fig. S1a). Mean winter (December-
 177 February) precipitation also has a positive correlation with spring GPP, ($r = 0.07$, $p = 0.77$, Fig. S1b), but it is much
 178 smaller than spring temperature. At interannual timescales, mean annual GPP shows a small increasing trend
 179 ($0.0072 \text{ g C m}^{-2} \text{ day}^{-1} \text{ per year}$) over the time period (Fig. S2), and largest correlation with winter (December –
 180 February) precipitation (Pearson's linear $r = 0.63$, $p = 0.003$, Fig. S3d) and shortwave irradiance ($r = -0.30$, $p = 0.22$,
 181 Fig. S3f). In contrast, spring temperature shows little correlation with mean annual GPP ($r = -0.02$, $p = 0.92$, Fig.
 182 S3c). It appears that winter precipitation and total irradiance are the dominant drivers in annual productivity, both of
 183 which are correlated, while spring temperature show a first order effect in driving spring GPP.

Deleted: in the traditional sense

Deleted: A

Deleted: B

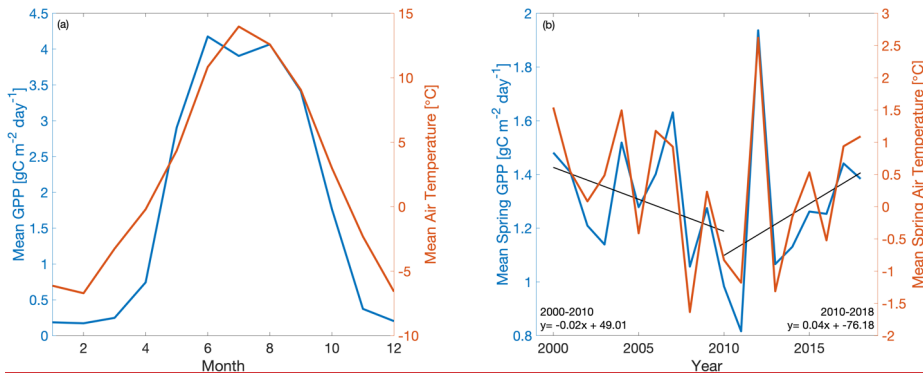
Deleted: A

Deleted: 1

Deleted: 2

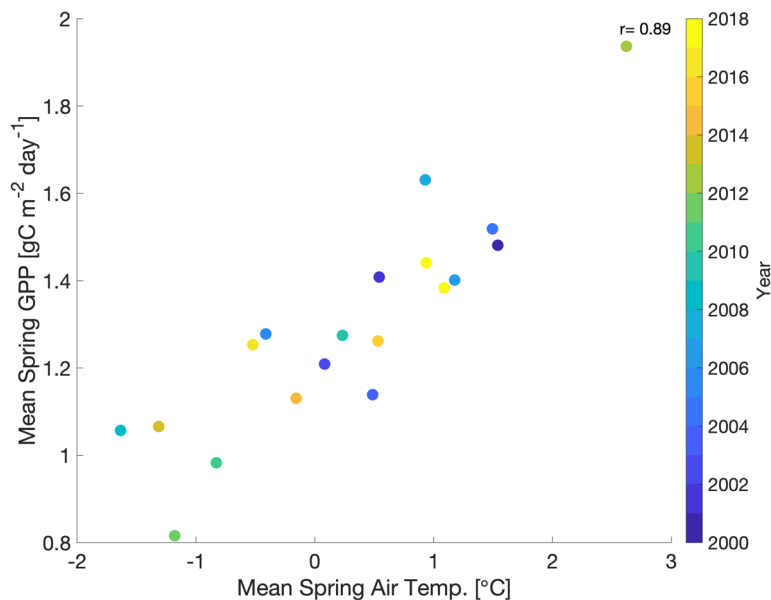
Deleted: 3

Deleted: s



184
 185 **Figure 1.** Time series of (a) mean monthly GPP (blue) and air temperature (orange) and (b) mean spring (March-May) GPP and
 186 air temperature at Niwot Ridge (US-NR1) from 2000-2018. GPP data are derived using a nighttime partitioning technique based
 187 on tower observations of NEE and air temperature.

198



199

200
201
202

Figure 2. Scatterplot of mean spring (March-May) GPP with mean spring air temperature with the **color bar** showing the corresponding year (2000-2018). 'r' is Pearson's correlation coefficient.

203

204

205

206

207

208

209

210

211

212

213

214

215

216

We also find that cold temperature has an important limitation on seasonal GPP at US-NR1. The seasonal cycle of GPP shows peak productivity in early summer (around June) and falling to near-zero values by early winter (November), continuing through late winter (February-March). Comparison of monthly GPP and minimum, maximum, and mean monthly air temperature shows an initiation of photosynthesis at monthly maximum air temperature above 0 °C (Fig. 3a) and monthly minimum air temperature above -5 °C (Fig. 3b). The strong dependence of monthly GPP on temperature is consistent with previous findings that temperature is an important driver of spring onset and seasonal variability of GPP in evergreen forests (e.g., Pierrat et al., 2021; Parazoo et al., 2018; Euskirchen et al., 2014; Armeth et al., 2006). As temperature falls in winter dormant plants, productivity becomes negligible. Productivity is triggered again when spring air temperature becomes warm enough to thaw stems, trigger xylem flow and promote access to soil moisture (e.g., Pierrat et al., 2021; Bowling et al., 2018; Ishida et al., 2001). Due to this observed dependence of GPP on temperature at US-NR1, we focus our analysis specifically on spring GPP, where we hypothesize that cold temperature is the dominant control on spring GPP variability.

Deleted: ~

Deleted: maximum

Deleted: in

Deleted: when sufficient radiation is available for absorption by green needles, and

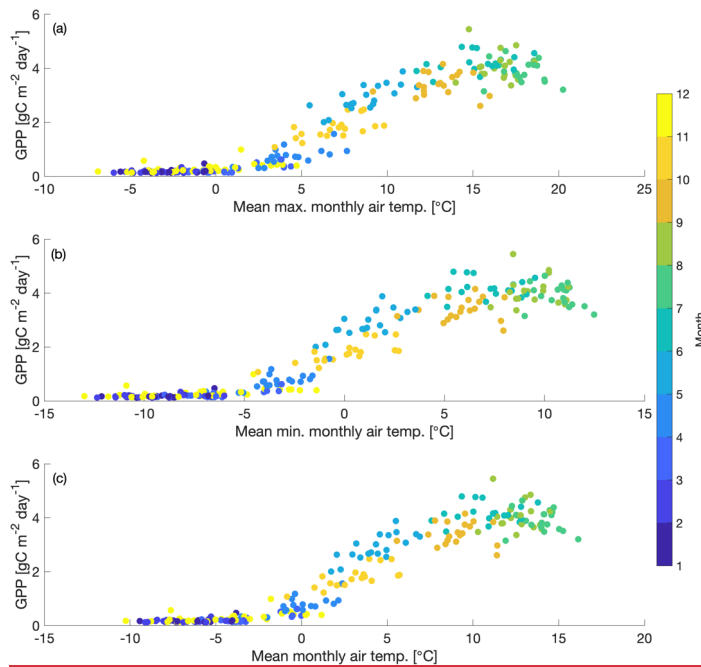


Figure 3. Scatter plot of mean monthly GPP vs. a.) mean maximum air temperature, b.) mean minimum air temperature and c.) mean air temperature for 2000-2018. Dots are colored with the corresponding month.

Deleted: average

In the baseline version of CARDAMOM, seasonal GPP in DALEC2 is limited primarily by incoming shortwave radiation. This light-focused limitation works well for deciduous forests where spring temperature and sunlight are correlated, as well as high latitude regions where sunlight is limited. However, for reasons discussed above, this method fails in evergreen forests such as Niwot Ridge whose green canopies are exposed to high sunlight and below-freezing temperature in spring. As temperature increases, evergreen stems slowly thaw, which enables the trees to access available soil moisture and slowly reactivate their carbon and water exchange processes (Mayr et al., 2014; Bowling et al., 2018). Temperature also impacts the reactivation of photosynthetic activity after winter dormancy (Öquist and Huner, 2003; Tanja et al., 2003). For example, fluctuating temperature in the spring has been shown to limit and sometimes reverse the activation of biochemical processes needed for photosynthesis recovery (Ensminger et al., 2004). Exposure to cold temperature, when combined with increased irradiance in the spring, can also damage evergreen trees (Öquist and Huner, 2003; Yang et al., 2020), therefore disrupting CO₂ assimilation. Previous studies have captured these cold temperature impacts at Niwot Ridge and other evergreen sites. For example, variations in photosynthetic pigments have been tied to seasonal temperature at Niwot Ridge (Magney et al., 2019). Pierrat et al. (2021) identified an increase in plant water flow (measured via changes in diurnal stem radius) and a change in carotenoid-chlorophyll ratios as temperature increases. The activation of water flow in the

242 evergreen trees, combined with the pigment changes to absorb more sunlight, allows for the recovery of
243 photosynthesis in the spring.

244 To represent the integrated impact of the cold weather processes, here we implement a cold temperature
245 scaling factor (g) in DALEC2. This scaling factor is developed by analyzing the relationship between monthly
246 minimum & maximum air temperature with tower-derived monthly GPP, where

247
$$\text{If: } T_{\min}(t) < T_0 : g = 0 \quad (1)$$

248
$$\text{If: } T_{\min}(t) > T_g : g = 1$$

249
$$\text{Else: } g(t) = \frac{(T_{\min}(t) - T_0)}{(T_g - T_0)}$$

250
$$\text{GPP}_{\text{cold}}(t) = \text{GPP}(t) * g(t) \quad (2)$$

251 $T_{\min}(t)$ is the observed minimum air temperature at Niwot Ridge at time t . $\text{GPP}(t)$ is the nominal ACM-based
252 DALEC2 GPP estimate (see section 2.3) and GPP_{cold} is the corresponding cold temperature GPP estimate. Equation
253 (2) may represent the integrated effect of all cold weather biophysical limitations, including processes such as the
254 impact of cold weather on plant hydraulics, and changes to carotenoid-chlorophyll ratios. We also theorize that our
255 temperature scaling factor partially captures soil moisture disruptions due to changing soil temperature. The
256 temperature thresholds in Eq. (1) may account for the connection between air temperature and soil temperature, with
257 initial and full soil thawing temperature potentially mirroring the photosynthesis shutdown and initiation air
258 temperature. CARDAMOM does not currently have explicit representations of soil moisture stress due to soil
259 freezing. Therefore, soil freezing stress and other biophysical processes impacted by cold temperature may be
260 approximated by this cold temperature scaling factor added to CARDAMOM. The temperature thresholds for
261 photosynthesis shutdown (referred to as T_0) and initiation (referred to as T_g) are added as model parameters in
262 DALEC2, bringing the total number of parameters to 35. These 35 DALEC parameters are simultaneously
263 optimized in CARDAMOM. The CARDAMOM Bayesian-inference probability distributions (see Appendix A) for
264 the T_0 (-7.1 ± 1.1 °C) and T_g (6.0 ± 2.6 °C) parameters used to define the cold temperature limitation are plotted in
265 Fig S4. We refer to the cold temperature constrained version of DALEC2 (within CARDAMOM) as DALEC2cold.

266 The baseline (DALEC2) and cold temperature (DALEC2cold) versions of the model are run for the 2000-
267 2018 period using tower observed, gap-filled, monthly meteorological (MET) drivers (including minimum and
268 maximum air temperature, shortwave radiation, vapor pressure deficit, and precipitation). We conduct four
269 experiments, summarized in Table 1: experiments using DALEC2 and DALEC2cold within CARDAMOM, where
270 19 years of GPP data are assimilated (referred to as CARD and CARDcold), and a corresponding pair of
271 experiments where only the first decade of data (2000-2009) is assimilated (referred to as CARD-Half and
272 CARDcold-Half) and the second decade of data (2010-2019) is withheld for validation, as a train-test scenario. All
273 months of GPP data are assimilated into the model, however our analysis focuses on the constraints on spring
274 (March-May) GPP. These four experiments serve to evaluate the sensitivity of modeled GPP at Niwot Ridge to cold
275 temperature limitation and parameter optimization. Specifically, the objective of experiments “CARD” and
276 “CARDcold” is to determine whether the cold temperature scaling factor improves the representation of spring GPP
277 variability across the 2000-2018 period; the objective of experiments “CARD-Half” and “CARDcold-Half” is to

Deleted: As such

Deleted: (1), to act as a thermostat that regulates evergreen
needleleaf carbon uptake phenology.

Deleted: where

Deleted: 3

Deleted: 1

Deleted: ,

Deleted: , and data assimilation

286 cross-validate the predictive skill of CARDcold by assessing whether the addition of a cold temperature scaling
 287 factor, informed by a subset of GPP data, can improve prediction of a withheld subset of GPP data.

Deleted: ¶

289 **Table 1.** Summary of CARDAMOM modeling experiments to determine sensitivity of seasonal and interannual spring GPP
 290 variability to cold temperature limitation (CARD vs CARDCold) and the ability to perform outside training window (Half).

Experiment Name	Met. Drivers	Time Period	GPP assimilation	Time period considered in assimilation	Uncertainties in GPP	Cold Temp. Limitation
CARD	yes	2000-2018	yes	2000-2018	20%	No
CARD-Half	yes	2000-2018	yes	2000-2009	20%	No
CARDCold	yes	2000-2018	yes	2000-2018	20%	Yes
CARDCold-Half	yes	2000-2018	yes	2000-2009	20%	Yes

291

292 2.5. Comparison to Terrestrial Biosphere Model Ensemble

293 A recent model intercomparison study provides an ideal benchmark for evaluating CARDAMOM
 294 simulations (section 2.4). Parazoo et al. (2020) conducted an experiment in which an ensemble of state-of-the-art
 295 terrestrial biosphere models (TBMs) were forced by the same observed meteorology at Niwot Ridge from 2000-2018,
 296 but with differences in spin-up, land surface characteristics, and parameter tuning. The TBMs are designed to simulate
 297 the exchanges of carbon, water, and energy between the biosphere and atmosphere, from global to local scales
 298 depending on inputs from meteorological forcing, soil texture, and plant functional type (PFT). The experiment was
 299 designed primarily to evaluate simulations of solar induced fluorescence (SIF) and GPP, the latter of which we focus
 300 on here. We refer the reader to Parazoo et al. (2020) for a more complete description of models, within-model
 301 experiments, and between-model differences.

302 The most important model differences worth noting here include the representation of stomatal conductance,
 303 canopy absorption of incoming radiation, and limiting factors for photosynthesis. We analyze a subset of the models
 304 which were run for multiple years, including SiB3 and SiB4 (Simple Biosphere model versions 3 and 4, respectively),
 305 ORCHIDEE (Organizing Carbon and Hydrology in Dynamic Ecosystems), BEPS (Boreal Ecosystems Productivity
 306 Simulator), and CLM4.5 and CLM5.0 (Community Land Model Versions 4.5 and 5.0, respectively). We also analyze
 307 within-model experiments in SiB3 and ORCHIDEE to isolate effects related to prescription of leaf area index (LAI;
 308 monthly varying in SiB3-exp1, fixed at 4.0 m²/m² in SiB3-exp2), temperature and water stress (ORCHIDEE-exp1
 309 includes temperature stress; ORCHIDEE-exp2 accounts for temperature and water stress), and data assimilation
 310 (ORCHIDEE-exp3, in which a subset of model parameters controlling photosynthesis and phenology are optimized

Deleted: -

Deleted: Ecosystems

314 against global OCO-2 SIF data, Bacour et al., 2019). Most of the TBM model experiments were run with default
 315 parameters (BEPS, CLM50, SiB3, SiB4, ORCHIDEE-exp1 and exp2). The other experiments were optimized in the
 316 following ways: either a) parameters were hand-tuned based on the US-NR1 data (CLM45) or b) the parameters were
 317 optimized using OCO-2 SIF data (ORCHIDEE-exp3). For more details on the parameterization of the TBM-SIF
 318 experiments, we refer the reader to Parazoo et al. (2020). The use of these models provides insight into the spread in
 319 model structures and the use of their default parameters. Finally, we note that not all model simulations span the entire
 320 observed record (2000-2018). While our analysis focuses on the long-term record from 2000-2018, we provide
 321 multiple comparisons to ensure consistency of time period: (1) IAV from 2001-2018 for SiB3, SiB4, ORCHIDEE,
 322 and CLM4.5; (2) IAV from 2012-2018 for SiB3, SiB4, ORCHIDEE, CLM4.5, and CLM5.0, and (3) seasonal
 323 variability from 2015-2018 for all models. We refer to the ensemble of models and within model experiments
 324 collectively as TBM-MIP.

Formatted: Font: Not Italic

Deleted: long term

Deleted: S

325 **3. Results & Discussion**

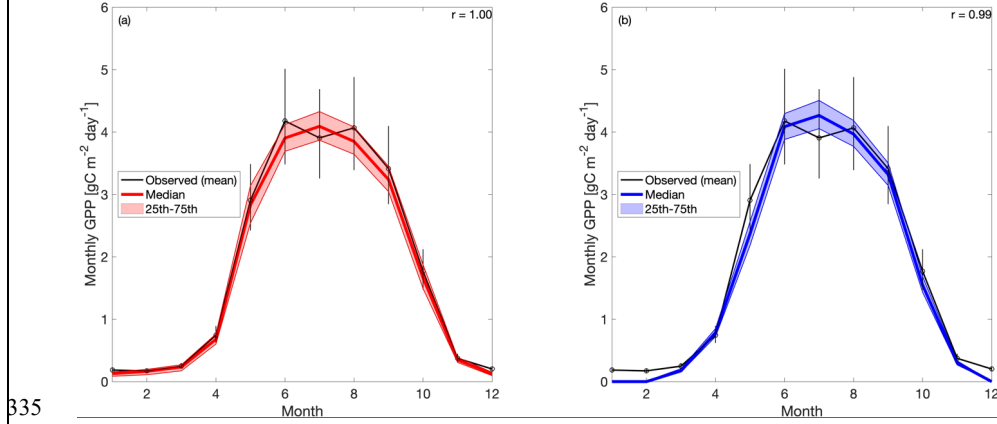
326 **3.1. Evaluation of CARDAMOM 2000–2018 GPP**

327 When the 19 years of tower-derived GPP data are assimilated into both versions of the model, the mean
 328 seasonal cycle is accurately replicated (Fig. 4). The Pearson's r values for CARD (Fig. 4a) and CARDcold (Fig. 4b)
 329 are almost equal ($r = 1.0$ and 0.99) with minimal increases in root mean square error (RMSE) and mean bias error
 330 (MBE) for CARDcold (RMSE = $0.24 \text{ g C m}^{-2} \text{ day}^{-1}$ and $0.23 \text{ g C m}^{-2} \text{ day}^{-1}$, MBE = $0.06 \text{ g C m}^{-2} \text{ day}^{-1}$ and 0.19 g C
 331 $\text{m}^{-2} \text{ day}^{-1}$ for CARD and CARDcold, respectively). Assimilating only the first decade of GPP data (Half
 332 experiments) does not drastically alter model performance (Fig. S5), with only slight changes in RMSE and MBE
 333 ($\Delta\text{RMSE} = 0.008 \text{ g C m}^{-2} \text{ day}^{-1}$, $\Delta\text{MBE} = 0.03 \text{ g C m}^{-2} \text{ day}^{-1}$ for CARD-Half, $\Delta\text{RMSE} = 0.003 \text{ g C m}^{-2} \text{ day}^{-1}$, ΔMBE
 334 $= 0.02 \text{ g C m}^{-2} \text{ day}^{-1}$ for CARDcold-Half).

Deleted: 4

Deleted: = 0.03

Deleted: = -



335

341 **Figure 4.** Tower-derived average monthly GPP (black line) and modeled GPP seasonal cycles at US-NR1, for 2000-2018, for a.)
342 CARD and b.) CARDcold experiments. The half-assimilation experiments (CARD-Half and CARDcold-Half) can be found in
343 the supplement (Fig S5). Model outputs include the median value of each experiment (bold color line) with the 25th-75th
344 percentiles of the ensembles (shaded area). The median is plotted instead of the mean to avoid impact of outlier ensemble
345 members (N = 4000). Error bars = tower-derived GPP multiplied/divided by $\exp(\sqrt{\log(2)^{2n}/n})$, n=# of years in average (n
346 = 19). 'r' is the Pearson's coefficient.

347
348 The cold experiments exhibit an improved fit to the observed IAV in spring productivity (Fig. 5), relative to
349 CARD, (r = 0.47, std = 0.03 g C m⁻² day⁻¹ for CARD; r = 0.88, std = 0.27 g C m⁻² day⁻¹ for CARDcold). CARDcold
350 also has slightly reduced RMSE (-0.01 g C m⁻² day⁻¹) and larger MBE (0.13 g C m⁻² day⁻¹). Similar to the seasonal
351 cycle analysis, the assimilation of only the first decade of GPP data (Half experiments) has minimal impact on
352 model performance (Δ RMSE = 0.007 g C m⁻² day⁻¹, Δ MBE = 0.06 g C m⁻² day⁻¹ for CARD-Half, and Δ RMSE =
353 0.02 g C m⁻² day⁻¹, Δ MBE = 0.02 g C m⁻² day⁻¹ for CARDcold-Half). We find less agreement between modeled and
354 tower-derived GPP IAV in summer for both CARD and CARDcold (CARD r = 0.32, std = 0.11 g C m⁻² day⁻¹;
355 CARDcold r = 0.05, std = 0.10 g C m⁻² day⁻¹; Fig. S6). While there is little variation in RMSE between the half and
356 full-assimilation experiments, RMSE is larger for summer than spring GPP (average RMSE = 0.23 g C m⁻² day⁻¹ for
357 spring model outputs, average RMSE = 0.35 g C m⁻² day⁻¹ for summer model outputs). Model agreement is further
358 reduced when considering annual average GPP (Fig. S7, Table S2). Although the cold temperature limitation
359 improves IAV slightly, it is still small compared to observed variability (mean annual std = 0.14 g C m⁻² day⁻¹).
360 Correlations to tower-derived GPP at the annual scale are small for both CARD and CARDcold (r = 0.19 and r =
361 0.22, Fig. S7a-b). Overall, the cold temperature limitation substantially improves agreement between the model and
362 tower-derived spring GPP, with slight reductions in performance for summer and annual GPP.

Deleted: , averaged

Deleted: 4

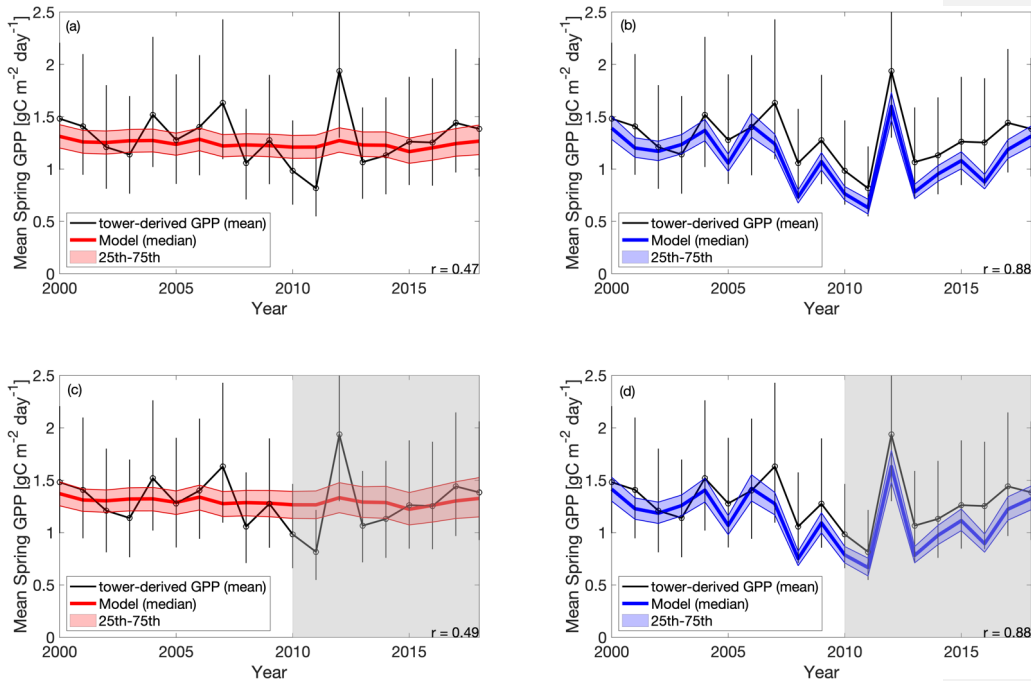
Deleted: 1

Deleted: 5

Deleted: 6

Deleted: 6

Deleted: :



371
372
373
374
375
376

Figure 5. Tower-derived (black line) mean spring (March-May) GPP with model interquartile range (shaded area) and median (bold color line) spring GPP outputs for a.) CARD, b.) CARDcold, c.) CARD-Half, and d.) CARDcold-Half experiments. The grey regions indicate no data assimilation (i.e. testing window). Model experiments are the same as in Figure 4. Uncertainty = $\exp(\sqrt{\log(2)^2 * n/n})$, $n = \#$ of months in average ($n = 3$).

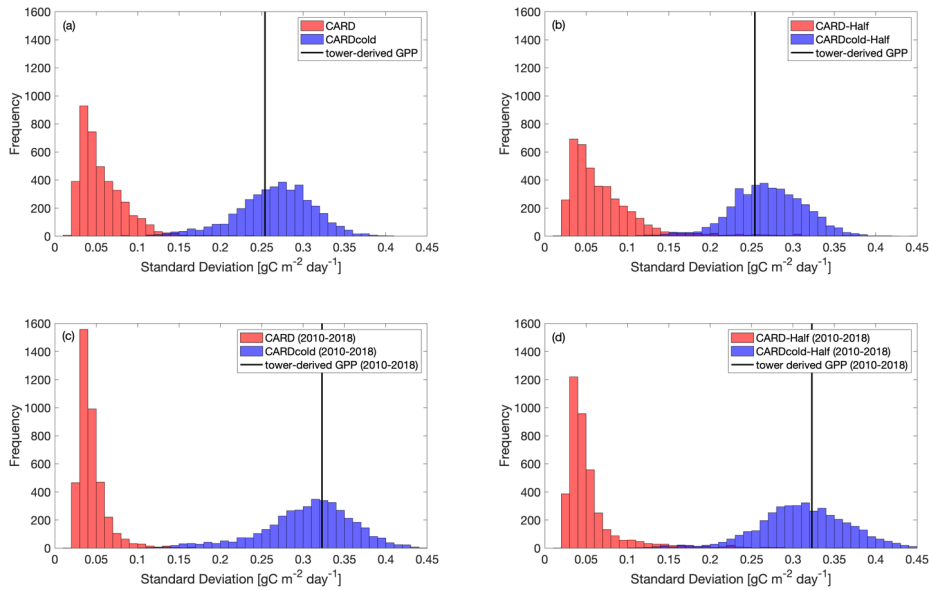
377
378
379
380
381
382
383
384
385
386
387

The standard deviation in tower-derived mean spring GPP (March-May) is approximately $0.25 \text{ g C m}^{-2} \text{ day}^{-1}$. The addition of the cold temperature limitation improves the model's ability to match the IAV of mean spring GPP (Fig. 6a-b). An examination of all modeled scenarios for CARD and CARDcold (i.e. all 4000 DALEC2 simulations), shows that the cold temperature limitation produces spring IAV values much closer to what is observed in the tower-derived GPP data. Only 0.3% of CARD ensembles produces mean spring IAV values within 20% of the tower-derived spring GPP standard deviation ($0.25 \pm 0.05 \text{ g C m}^{-2} \text{ day}^{-1}$), whereas 69% of CARDcold ensembles have standard deviation values within the same range. Interestingly, assimilating only the first ten years of GPP data (Half experiments, Fig. 6b) slightly increases the number of ensemble members with standard deviations within the mentioned range for both CARD-Half (2.4%) and CARDcold-Half (70%). It is promising to see that despite not assimilating the 2010-2018 GPP data into the model, CARDcold-Half is still able to match average spring IAV of the full data record.

388
389
390

We also consider the IAV in spring GPP for just the second half of the data record (2010-2018). IAV of tower-derived spring GPP increases slightly in 2010-2018 ($0.32 \text{ g C m}^{-2} \text{ day}^{-1}$). Once again, the cold temperature limitation enables CARDAMOM to match spring GPP IAV (Fig. 6c-d). 0.03% of CARD ensembles produce mean

391 spring IAV values within 20% of the tower-derived spring GPP standard deviation for the 2010-2018 period ($0.32 \pm$
 392 $0.06 \text{ g C m}^{-2} \text{ day}^{-1}$), whereas 76% of CARDcold ensembles have standard deviation values within the same range.
 393 For the Half experiments, 0.6% of CARD and 75% of CARDcold ensembles have IAV values within 20% of the
 394 standard deviation for 2010-2018. **This improvement in matching IAV is also observed when considering mean**
 395 **annual GPP (Fig. S8), but is much smaller than the improvements made for spring GPP.** Overall, CARDcold
 396 produces a less biased distribution of IAV values (relative to both assimilated and withheld observations), whereas
 397 CARD is more skewed towards smaller IAVs, which indicates that the cold temperature limitation enables a
 398 mechanistic and statistical improvement in capturing the interannual variability of spring GPP.
 399



400
 401 **Figure 6.** Histograms comparing standard deviation in mean spring GPP across all ensembles ($N=4000$) for CARD (red bars) and
 402 CARDcold (blue bars) experiments with a.) full assimilation, b.) half assimilation, c.) full assimilation for the second decade
 403 (2010-2018), and d.) half assimilation for the second decade (2010-2018). Black line indicates standard deviation in tower-
 404 derived mean spring GPP (std = $0.25 \text{ gC m}^{-2} \text{ day}^{-1}$ for full period (a-b), std = $0.32 \text{ gC m}^{-2} \text{ day}^{-1}$ for 2010-2018 (c-d)).
 405

406 **3.2. Temperature controls on springtime GPP**

407 The added value of the DALEC2 cold temperature limitation for modeling mean spring (March-May) GPP
 408 is logically due to large fluctuations in spring temperature at Niwot Ridge. The cold temperature limitation allows
 409 DALEC2-CARDAMOM to match the IAV of spring tower-derived GPP closely. Furthermore, the cold temperature
 410 limitation enables the model to match tower spring IAV in the second half of the time period (2010-2018) when only
 411 the first ten years of GPP data are assimilated (2000-2009). This indicates that the cold temperature limitation is

Deleted: 1

413 able to estimate spring GPP outside of its training window and could be useful at other sites where data availability
414 is limited. Future work will include evaluating the cold temperature limitation at other sites to ensure that it is
415 applicable beyond Niwot Ridge, for example using forecast skill metrics proposed by Famiglietti et al. (2021).

416 Temperature-induced spring onset of GPP is driven by two general processes: (1) initiation of bud burst
417 and leaf expansion leading to increasing LAI, and/or (2) initiation of photosynthetic activity (photosynthetic
418 efficiency i.e., GPP per unit of LAI) due to temperature-induced changes in plant hydraulics (Ishida et al., 2001;
419 Pierrat et al., 2021) or kinetics of the photosynthetic machinery (e.g., Medlyn et al., 2002). In situ LAI
420 measurements suggest that the LAI at Niwot Ridge is relatively constant across the season, which is somewhat
421 expected given the dominant tree species at the site. Hence, the temperature-induced onset of GPP is likely due to
422 the latter process, increased photosynthetic efficiency, as supported by the measurements (Figs. 1-2), although small
423 changes in LAI are still feasible given uncertainties in the measurements. The inclusion of the cold temperature
424 limitation scaling factor in the model, a semi-empirical process, leads to a substantial improvement in model
425 representation of GPP at the site. Further development may also look to identify the relative roles of increased LAI
426 and increased photosynthetic efficiency at Niwot Ridge and other evergreen needleleaf sites, as changes in GPP can
427 lead to changes in carbon allocation to LAI, among other plant carbon pools.

428 Temperature is important in both the reactivation of photosynthetic activity in the spring and the wind
429 down of productivity in the fall (Flynn and Wolkovich, 2018; Stinziano and Way, 2017). Therefore, we anticipate
430 that the cold temperature scaling function may also improve our ability to model fall productivity. However, other
431 factors such as water availability and photoperiod must also be considered (Bauerle et al., 2012; Stinziano et al.,
432 2015). Future studies at Niwot Ridge and other sites should investigate the role of these factors (temperature, water,
433 photoperiod) in regulating fall GPP and how we can represent these processes in CARDAMOM.

434 With the inclusion of the cold temperature limitation on GPP and its application in CARDAMOM, we
435 provide a data-constrained estimate of the climate sensitivity of the Niwot Ridge forest to spring temperature.
436 Posterior estimates indicate that GPP is gradually inhibited below $6.0\text{ }^{\circ}\text{C} \pm 2.6\text{ }^{\circ}\text{C}$ (T_c) and completely inhibited
437 below $-7.1\text{ }^{\circ}\text{C} \pm 1.1\text{ }^{\circ}\text{C}$ (T_0). The gradual limitation of GPP by temperature has been observed on hourly and daily
438 timescales in other cold-weather ecosystems, such as Alaskan conifers (Parazoo et al., 2018) and Canadian spruce
439 (Pierrat et al., 2021). This has been connected to the triggering of transpiration and water flow from xylem into
440 leaves (Ishida et al., 2001). However, both biotic (e.g., carotenoid/chlorophyll ratios) and abiotic (e.g., openness of
441 canopy) factors together regulate GPP response to meteorological forcings, and further process-oriented
442 investigations are required to resolve the emergent response of GPP to temperature. Furthermore, the use of
443 process-based models will be needed to disentangle the individual cold weather biophysical processes currently
444 represented in the scaling factor (Eq. 1-2). For now, this is a useful metric for climate-sensitivity of spring GPP, at
445 least in the absence of long-term adaptations. Furthermore, over the 19 year observation period investigated here the
446 use of a temporally constant T_0 and T_c yields significantly improved GPP estimates, suggesting that much of the
447 variability can be attributed to climate-driven changes, not interannual variation in vegetation parameters. As
448 temperature continues to increase due to climate change (particularly in the early growing season), productivity at
449 US-NRI could increase as a result and therefore increase carbon uptake, with productivity peaking earlier in the

Deleted: 0

451 [year \(e.g., Xu et al., 2016\). However, these spring gains in GPP have been shown to not offset the losses of carbon](#)
452 [due to summer droughts \(e.g., Buermann et al., 2013; Knowles et al., 2018\). It is also unclear how the long-term](#)
453 [stress of increased temperature could affect forest productivity directly.](#)

454 This study [focuses](#) on the relationship between temperature and GPP and its usefulness on model
455 predictions of spring GPP, but an important component that cannot be ignored is the confounding effect of water
456 availability on GPP. Future changes in winter precipitation are more uncertain, therefore limiting our ability to
457 analyze how precipitation changes will alter future productivity. While precipitation observations [are](#) analyzed to
458 discern any major connections between GPP and meteorological controls, an analysis of how precipitation affects
459 model predictability [is](#) not included in this study. The combined results, including the cold temperature limitation
460 and train-test data assimilation experiments, suggest that other factors besides spring temperature, most notably
461 winter and summer precipitation (Fig. [S3](#)) and resulting soil water limitation, also have important impacts on
462 summer GPP. We therefore highlight the need to jointly resolve springtime temperature limitation, in conjunction
463 with water stress limitations in future efforts to understand the integrated role of environmental forcings on
464 interannual GPP variability. Furthermore, this analysis [does not](#) consider how winter precipitation as snowfall
465 versus rainfall affects [s](#) productivity, or how resulting changes to winter snowpack could alter productivity long-term.
466 Since annual average GPP appears to be more dependent on winter precipitation/snowpack ([Pearson's linear r =](#)
467 [0.63, Fig. S3a](#)), future work will include improving model predictability of late season productivity and quantifying
468 temperature-water effects on carbon uptake. The definition of the seasons could also alter the connections drawn
469 between seasonal temperature, precipitation and productivity.

470 3.3. Model intercomparison and implications for GPP models

471 Here, we evaluate DALEC2-CARDAMOM against mean spring GPP estimates from TBM-MIP models
472 (Section 2.5 and Parazoo et al. 2020). It is important to remind the reader that the CARDAMOM runs have a
473 significant advantage over the TBM-MIP models in this analysis, as CARDAMOM is trained on US-NR1 GPP data.
474 While TBM-MIP models use tower-observed meteorological inputs, prescribe tower-specific and time-invariant
475 structural properties such as LAI observed at US-NR1 (SiB3-exp2 [and](#) CLM4.5), and use data assimilation of global
476 remote sensing data to constrain globally representative plant functional types (ORCHIDEE-exp3), they are not
477 directly constrained by time-varying carbon fluxes at the tower. As such, we emphasize that our model comparison
478 is not a [strict assessment of performance](#), but rather an attempt to [learn how model simulation of GPP at an](#)
479 [evergreen needleleaf site can be improved.](#)

480 [There is a wide range in performance of TBM-MIPs in representing the magnitude and IAV of tower-](#)
481 [derived spring GPP \(Figure 7a\).](#) Pearson's r correlations range from 0.25 to 0.82 (mean $r = 0.6$, [Table 2](#)) from 2001-
482 2018, with the same models showing slightly improved performance over the second decade (mean $r = 0.73$ from
483 2012-2018). ORCHIDEE-exp1 and CLM4.5 show consistently high performance over all three periods analyzed,
484 with CLM5.0 excelling from 2012-2018, and BEPS from 2015-2018 (Table S1). CLM4.5 also shows [the](#) smallest
485 mean bias of the TBM-MIP models (RMSE ~ 0.35), and high agreement in the magnitude of spring GPP variability
486 (1-sigma standard deviation = $0.21 \text{ g C m}^{-2} \text{ day}^{-1}$ for CLM4.5, vs $0.25 \text{ g C m}^{-2} \text{ day}^{-1}$ observed). While

Deleted: 2

Deleted: s

Deleted: ed

Deleted: &

Deleted: -

Deleted: competition

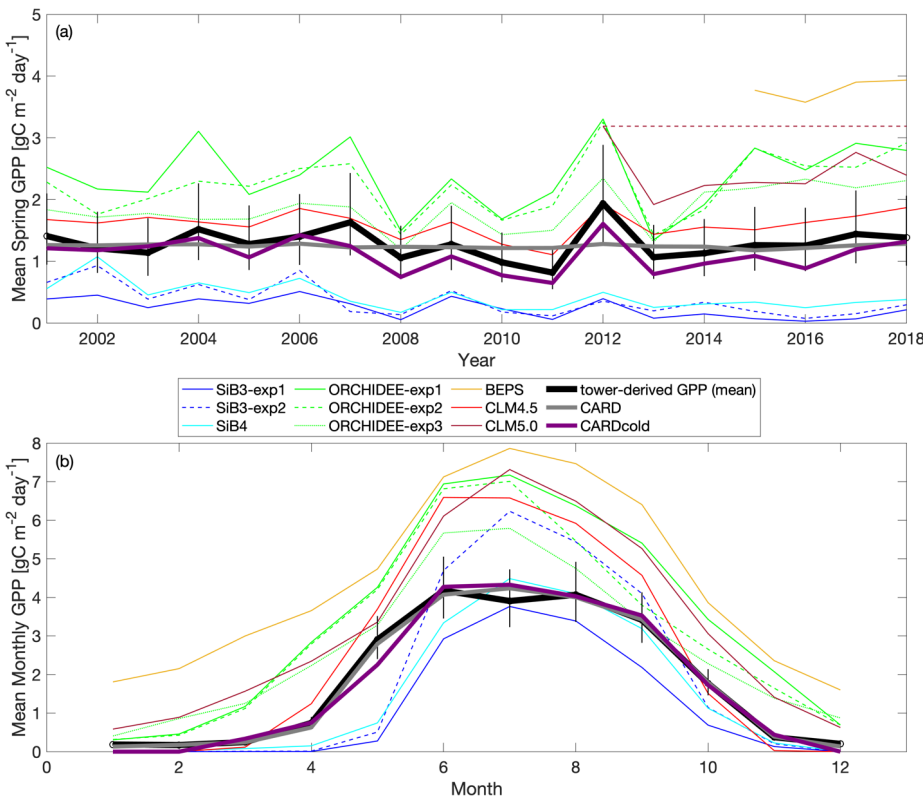
Deleted: discern common environmental controls in model performance of simulating the magnitude and seasonal-to-interannual variability of spring GPP at an evergreen needleleaf site...

497 acknowledging the advantage of data assimilation, it is promising to see that CARDAMOM (with the addition of the
 498 cold temperature limitation) is able to perform comparably to the TBM-MIP models. In particular, CARDcold is
 499 well correlated in the direction ($r = 0.88$) and magnitude (1-sigma ~ 0.26) of interannual variability, as well as overall
 500 magnitude of spring GPP (low RMSE and MBE).

501 The range of performance across within-model experiments reveals important processes, and uncertainty of
 502 process representation, in driving the magnitude and variability of spring GPP. For example, the ORCHIDEE data
 503 assimilation experiment (exp3) shows consistently and substantially lower overall correlation (e.g., $r = 0.59$ from
 504 2001-2018) than corresponding free running experiments (exp 1 and 2, $r = 0.78-0.82$), but has reduced RMSE and
 505 MBE (RMSE = $0.63 \text{ g C m}^{-2} \text{ day}^{-1}$ vs $1-1.14 \text{ g C m}^{-2} \text{ day}^{-1}$). Likewise in SiB3, prescribing an empirically-based but
 506 fixed-in-time LAI of $4.0 \text{ m}^2/\text{m}^2$ (exp2) reduces mean bias, but degrades variability ($r = 0.25$) compared to time-
 507 variable LAI (exp1) prescribed from satellite data ($r = 0.50$).

508
 509

Formatted: Superscript
 Formatted: Superscript



510
 511

512 **Figure 7.** Comparison of TBM-MIP models to CARD and CARDcold experiments for a.) mean spring GPP for 2000-2018 and
 513 b.) monthly GPP from 2015-2018. Note that fill values are ignored when calculating mean annual values for TBM-MIP
 514 experiments. Uncertainty = $\exp(\sqrt{\log(2)^2 * n/n})$, where n = # years in average (n = 19).
 515

Deleted: and b.

516 There is also large variability in the modeled seasonal cycle (Fig. 7b) and mean annual GPP (Fig. S9). For
 517 mean annual GPP estimates, Pearson's r values are reduced for all models (Table S2). Once again, ORCHIDEE-
 518 exp2 and ORCHIDEE-exp3 stand out with some of the higher correlations ($r = 0.60$ and $r = 0.64$) and p-values
 519 below 5% significance level. Furthermore, ORCHIDEE-exp3 (temperature stress with SIF data assimilation) has
 520 the lowest RMSE and MBE of the model set. SiB3-exp2 (fixed LAI) has a standard deviation closest to
 521 "observations" ($0.14 \text{ gC m}^{-2} \text{ day}^{-1}$), and the smallest RMSE and MBE of the TBM models.

Deleted: 7

522 Most TBM-MIP models capture the shape of the seasonal cycle at Niwot Ridge. For the 2015-2018 period,
 523 all models have Pearson's r values larger than 0.91, with p-values much smaller than a 5% significance level (Table
 524 S3). With the help of data assimilation, CARDcold accurately captures the seasonal cycle at Niwot Ridge with
 525 reduced error (RMSE = $0.22 \text{ g C m}^{-2} \text{ day}^{-1}$, MBE = $0.07 \text{ g C m}^{-2} \text{ day}^{-1}$), and data assimilation experiments in
 526 ORCHIDEE-exp3 show reduced bias relative to free running experiments. The cold temperature limitation has little
 527 impact on the modeled mean seasonal cycle or mean annual GPP estimates in CARDAMOM, and appears to be
 528 most valuable for improving spring GPP variability.
 529

530 **Table 2.** Pearson's linear r, R-squared, p-value, standard deviation, root mean square error (RMSE), and mean bias error (MBE)
 531 for TBM-MIP and all CARDAMOM experiments to Niwot Ridge tower-derived mean spring (March-May) GPP. Open values
 532 reflect statistics for the 2001-2018 period, while values in parentheses represent the 2012-2018 period. All relevant statistics are
 533 calculated at 5% significance level. *BEPs statistics are not included in this table as this model only has GPP estimates for 2015-
 534 2018.

model	r-value	R-squared	p-value ($\alpha = 0.05$)	RMSE ($\text{gC m}^{-2} \text{ d}^{-1}$)	MBE ($\text{gC m}^{-2} \text{ d}^{-1}$)	standard deviation ($\text{gC m}^{-2} \text{ d}^{-1}$)
CARD-Half	0.47 (0.55)	0.22 (0.30)	0.05 (0.20)	0.24 (0.26)	-0.005 (0.06)	0.03 (0.04)
CARD	0.45 (0.57)	0.20 (0.33)	0.06 (0.18)	0.24 (0.28)	0.05 (0.12)	0.03 (0.04)
CARDcold-Half	0.88 (0.93)	0.77 (0.86)	0.00 (0.002)	0.21 (0.24)	0.17 (0.22)	0.26 (0.29)
CARDcold	0.87 (0.93)	0.76 (0.87)	0.00 (0.00)	0.23 (0.26)	0.20 (0.24)	0.26 (0.28)
SiB3-exp1	0.50 (0.81)	0.25 (0.66)	0.04 (0.03)	1.07 (1.23)	1.04 (1.21)	0.16 (0.13)
SiB3-exp2	0.25 (0.41)	0.06 (0.17)	0.32 (0.36)	0.97 (1.15)	0.92 (1.13)	0.26 (0.10)
SiB4	0.34 (0.91)	0.12 (0.83)	0.16 (0.00)	0.90 (1.04)	0.86 (1.02)	0.22 (0.09)
ORCHIDEE-exp1	0.82 (0.82)	0.68 (0.67)	0.00 (0.02)	1.14 (1.24)	-1.08 (-1.16)	0.56 (0.67)
ORCHIDEE-exp2	0.78 (0.79)	0.61 (0.63)	0.00 (0.03)	1.00 (1.20)	-0.95 (-1.12)	0.51 (0.64)
ORCHIDEE-exp3	0.59 (0.55)	0.35 (0.31)	0.01 (0.20)	0.63 (0.81)	-0.57 (-0.76)	0.35 (0.36)
BEPS*	X	X	X	X	X	X
CLM4.5	0.82 (0.85)	0.68 (0.73)	0.00 (0.01)	0.34 (0.35)	-0.31 (-0.31)	0.21 (0.18)
CLM5.0	(0.96)	(0.92)	(0.00)	(1.09)	(-1.08)	(0.42)

535
 536 In summary, TBM-MIP experiments reveal several key factors that can improve or degrade estimates of
 537 spring GPP at Niwot Ridge. For example, adapting model parameters to needleleaf species based on hand-tuning to

540 tower data and formal data assimilation methods (CLM4.5 and ORCHIDEE-exp3, respectively) improves the
541 overall magnitude of spring GPP. Likewise, prescribing LAI to a constant value of 4.0 m²/m² based on tower
542 measurements (SiB3-exp2) improves year-to-year variability, while prescribing time variable LAI based on MODIS
543 data improves spring GPP magnitude (SiB3-exp1). SiB4, which has prognostic rather than prescribed phenology,
544 represents a compromise in magnitude and variability when looking at the entire record (2001-2018), but is one of
545 the top performers across all TBM-MIP models over the most recent period (2012-2018).

546 We did not directly consider changes in canopy structural or biophysical characteristics in our
547 CARDAMOM experiments. In CARDAMOM, LAI is a prognostic quantity (a function of foliar C and leaf carbon
548 mass per area). In the absence of LAI observational constraints, CARDAMOM LAI is indirectly informed by the
549 constraints of time-varying GPP on DALEC2 parameters (see section 2.3). Our results suggest that additional
550 improvements are possible with careful consideration of in situ measured vegetation parameters.

551 TBM-MIP experiments also offer insight on important environmental controls and process representation.
552 Air temperature is an effective constraint of spring GPP onset (CLM4.5, ORCHIDEE-exp1, Figure 7 and Table 2),
553 but which can be degraded when large scale data assimilation does not account for local- to regional- vegetation
554 characteristics in parameter optimization (e.g., ORCHIDEE-exp3, Table 2). Water availability appears to be a
555 secondary but still important driver of spring GPP. While acknowledging the numerous differences between
556 CLM4.5 and CLM5.0, we find it important to note that plant hydraulic water stress (CLM5.0) shows improved IAV
557 performance (high correlation, Table 2) over simplified soil moisture stress functions (CLM4.5). This result further
558 supports efforts to closely analyze seasonal GPP to locate different environmental controls for future model
559 improvements.

560 Our study of the controls of cold temperature on GPP has important implications for modeling seasonal
561 productivity. First, future work must evaluate cold temperature limitation at other sites across an array of ecosystem
562 types. Additionally, it is important to determine if the temperature thresholds of photosynthesis initiation and
563 cessation are similar across locations, or unique to ecosystem type and/or site. Previous studies have had mixed
564 results, supporting both the use of customized temperature threshold parameters dependent on the site (Tanja et al.,
565 2003; Chang et al., 2020) or for a general parameter across multiple sites or biome type (Bergeron et al., 2007).
566 These differences could be due to variations in other variables (e.g., soil temperature, irradiance, etc.) and/or
567 physiological differences in the vegetation species. Identifying how photosynthesis temperature thresholds vary
568 across space and ecosystem type would be beneficial in improving model performance in simulating productivity.
569 Our model intercomparison study also provide insights on how we may improve our ability to model seasonal GPP.
570 For example, in Fig. 7b, we see that the ORCHIDEE model growing season starts too early. In the photosynthesis
571 module of ORCHIDEE, the temperature-dependency of parameters are described by Arrhenius or modified
572 Arrhenius functions following Medlyn et al. (2002) and Kattge and Knorr (2007). In general, the functions are used
573 to estimate the potential rates of Rubisco activity and electron transport based on temperature, as these rates are
574 needed to determine photosynthetic capacity (Medlyn et al., 2002). The lowest temperature for productivity
575 mentioned in these studies are 5°C and 11°C, respectively. Additionally, there is a test at the start of the
576 photosynthesis subroutine that prevents the computation of photosynthesis if the mean temperature over the last 20

Deleted: 1

Deleted: spring GPP magnitude,

Deleted: year-to-year variability

Deleted: 2

Deleted: I

Deleted: -

Deleted: and reduced error

584 days falls below -4°C. For our study, the only ORCHIDEE experiment that uses specific data related to the plant
585 functional type of this site (OCO-2 SIF data for US-NR1) is ORCHIDEE-exp3. This experiment improves the
586 general behavior of the modeled GPP seasonal cycle but does not improve ORCHIDEE's ability to capture the start
587 of the growing season. So with the future evaluation of cold temperature limitation at other sites and further study of
588 the potential temperature-influenced bias in the model, then ORCHIDEE (and other process-based models) may
589 need to improve its photosynthesis temperature-dependency for cold plant functional types. Therefore, we
590 recommend implementing a cold temperature GPP limitation in a process-based model to confirm its ability to
591 improve model performance. If we identify (1) how photosynthesis initiation and shutdown varies with temperature
592 and location, and (2) apply a cold temperature limitation successfully in a process-based model, then we could
593 expand our analyses to answer bigger Earth science questions. For example, we could use Earth System Model
594 temperature trends to determine how changing temperature will impact GPP in the future.

595 While further experiments are needed, these results demonstrate the value of (1) site-level data assimilation
596 for local scale prediction of GPP magnitude and variability, (2) global data assimilation for reducing magnitude
597 biases, and (3) process formulation for accounting for sensitivity to temperature limitation and water stress. Overall,
598 these results are encouraging for model-data fusion systems which have developed the capacity to bring together
599 temporally and spatially resolved functional and structural vegetation components such as LAI, SIF, soil organic
600 matter, and above- and below-ground biomass (e.g., Bacour et al., 2019; Smith et al., 2020; Bloom et al., 2020).
601 Joint assimilation of these datasets, coupled with observed meteorological forcing, has potential to introduce more
602 emergent constraints of vegetation change with respect to environmental change, thus improving overall estimates of
603 productivity. Future work will assess the joint impact of SIF, ET, LAI, and biomass data as effective constraints on
604 light use and water use efficiency (Smith et al., 2020), which is expected to improve the ability of CARDAMOM to
605 use light with respect to increasing biomass subject to longer growing seasons and heat and water stress.

606 4. Conclusions

607 Despite mechanistic advances in ecosystem modeling, it is still a challenge to simulate temporal variations
608 in GPP. In an attempt to dissect the environmental controls on GPP in an evergreen needleleaf ecosystem, we
609 analyzed the impact of temperature on spring (March-May) productivity by implementing a cold temperature GPP
610 limitation within a model-data fusion system (DALEC2-CARDAMOM). The cold weather GPP limitation allows
611 for improved model estimates of mean spring productivity at Niwot Ridge, specifically CARDAMOM's ability to
612 match the interannual variability observed in tower-derived mean spring GPP. Furthermore, CARDAMOM is able
613 to match spring interannual variability between model and tower data outside of the training period. When
614 compared to TBM-MIP models, controls that appear to impact model performance include the inclusion of water
615 stress (e.g., soil moisture) and vegetation parameters (e.g., prescription of LAI). The fact that the cold temperature
616 limitation does not improve CARDAMOM's annual GPP estimates suggests that other controls (i.e. winter
617 precipitation) drive GPP variability in other parts of the year, most likely summer (June-September). The cold
618 temperature limitation may prove useful in understanding future changes in spring productivity due to changes in
619 temperature in other ecosystems as well.

Deleted: -

Deleted: e.g.

Deleted: important ecosystems, such as the Western U.S

623 **Appendices**

624 **Appendix A: Model-Data Fusion Methodology**

625 The DALEC2 model parameter values and state variable initial conditions (henceforth \mathbf{x}) are optimized
626 using a Bayesian inference approach, where the posterior probability distribution of \mathbf{x} given observations \mathbf{O} , $p(\mathbf{x}|\mathbf{O})$,
627 can be expressed as

628
$$p(\mathbf{x}|\mathbf{O}) \propto p(\mathbf{x})L(\mathbf{x}|\mathbf{O}) \tag{A1}$$

629 Where $p(\mathbf{x})$ is the prior probability distribution of \mathbf{x} , and $L(\mathbf{x}|\mathbf{O})$ is the likelihood of the DALEC parameters
630 and initial conditions given observations \mathbf{O} . We define the likelihood function as

631
$$L(\mathbf{x}|\mathbf{O}) = e^{-\frac{1}{2}\sum_i \left(\frac{m_i(\mathbf{x}) - o_i}{\sigma}\right)^2} + e^{-\frac{1}{2}\sum_a \left(\frac{m'_a(\mathbf{x}) - o'_a}{\sigma'}\right)^2}, \tag{A2}$$

632
633 where for monthly timestep i , $m_i(\mathbf{x})$ and o_i represent monthly modeled GPP (based on parameters \mathbf{x}) and
634 flux-tower GPP observation, respectively. Following model-data fusion efforts with a spectrum of temporal modes
635 of variability (Desai 2010, Quetin et al., 2020 and Bloom et al., 2020), we extend the cost function to include mean
636 annual model and tower-derived GPP, $m'_a(\mathbf{x})$ and o'_a respectively) for year = a , which allows the GPP cost function
637 to be sensitive to both seasonal and inter-annual components of the flux tower GPP signal. We log-transform
638 modeled and tower-derived GPP values (as done in Bloom & Williams, 2015 and Bloom et al., 2016), which is
639 preferable for characterize model-data residuals between strictly positive quantities (such as GPP). For lack of better
640 uncertainty estimates on monthly and annual flux tower GPP accuracy—including lack of knowledge on GPP error
641 characteristics at monthly timescales, error covariance between individual GPP estimates, model structural error
642 impacts on GPP—we conservatively prescribed uncertainty factor of $\sigma = 2$ for monthly values (roughly ~75%), and
643 $\sigma' = 1.2$ (~18%) for annual values; in general we found that these values led to robust agreements between flux
644 tower and DALEC2 GPP variability (model-data mismatch metrics are reported in section 3 of the manuscript).

645 For all model experiments, we sample the probability of $p(\mathbf{x}|\mathbf{O})$, the posterior probability distribution of
646 initial conditions \mathbf{x} given observations \mathbf{o} , we use four Metropolis-Hastings Markov Chain Monte Carlo (MHMCMC;
647 Haario et al. 2001) for 10^8 iterations; we subsample 1000 parameter vectors \mathbf{x} , from the latter 50% of each chain (in
648 total 1000 samples x 4 chains = 4000 samples). We test for convergence in the MHMCMC estimates of \mathbf{x} using a the
649 Gelman-Rubin convergence diagnostic to measure convergence between the four chains.

650 **Data Availability**

651 The Ameriflux US-NR1 data were obtained from: <https://ameriflux.lbl.gov/sites/siteinfo/US-NR1> (Blanken et al.,
652 2020). The US-NR1 data used in this study, as well as the CARDAMOM and TBM-MIP outputs are publicly
653 available and provided in .nc file format at <http://doi.org/10.5281/zenodo.4928097>.

Deleted: 1

Deleted: 1

Deleted: as

657 **Code Availability**

658 [The CARDAMOM code used in this study is available here: https://github.com/CARDAMOM-](https://github.com/CARDAMOM-framework/CARDAMOM_v2.2)
659 [framework/CARDAMOM_v2.2](https://github.com/CARDAMOM-framework/CARDAMOM_v2.2)

660 **Author Contributions**

661 SGS, NCP and AAB designed and performed the research. AJN, BR, CB, FM, IB, YZ, BQ, and MS contributed
662 model simulations. DRB, SPB, and PDB contributed observational data. All authors contributed to the writing of
663 the paper [and/or revision of the manuscript](#).

664 **Supplement**

665 **Competing Interests**

666 [An author is a member of the editorial board of *Biogeosciences*. The peer-review process was guided by an](#)
667 [independent editor, and the authors have also no other competing interests to declare.](#)

668 **Acknowledgements**

669 [The US-NRI AmeriFlux site has been supported by the U.S. DOE, Office of Science through the AmeriFlux](#)
670 [Management Project \(AMP\) at Lawrence Berkeley National Laboratory under Award Number 7094866.](#) A portion
671 of this research was carried out at the Jet Propulsion Laboratory, California Institute of Technology, under contract
672 with NASA. Funding from the NASA Earth Science Division Arctic Boreal Vulnerability Experiment (ABOVE) is
673 acknowledged. We acknowledge the MEASUREs program. [SGS was partly supported by a University of California,](#)
674 [Irvine graduate student fellowship.](#) DRB and BMR were supported by the NASA CMS (80NSSC20K0010) and the
675 [NSF Macrosystems Biology and NEON-Enabled Science \(1926090\) Programs.](#) The National Center for
676 [Atmospheric Research \(NCAR\) is sponsored by NSF.](#) MS was partly supported by the U.S. Department of Energy
677 [Office of Science Biological and Environmental Research as part of the Terrestrial Ecosystem Science Program](#)
678 [through the Next-Generation Ecosystem Experiments \(NGEE\) Tropics project.](#) PNNL is operated by Battelle
679 [Memorial Institute for the U.S. DOE under contract DE-AC05-76RLO1830.](#)

680 **References**

681 Anav, A., Friedlingstein, P., Beer, C., Ciais, P., Harper, A., Jones, C., Murray-Tortarolo, G., Papale, D., Parazoo, N.
682 C., Peylin, P., Piao, S., Sitch, S., Viovy, N., Wiltshire, A., and Zhao, M.: Spatiotemporal patterns of terrestrial gross
683 primary production: A review, *Rev. Geophys.*, 53, 785–818, <https://doi.org/10.1002/2015RG000483>, 2015.
684
685 Armeth, A., Lloyd, J., Shibistova, O., Sogachev, A., and Kolle, O.: Spring in the boreal environment: observations on
686 pre- and post-melt energy and CO₂ fluxes in two central Siberian ecosystems, *Boreal Environ. Res.*, 11, 311–328,
687 2006.
688

Deleted: ¶

Formatted: Heading 1

Formatted: Font: Italic

Deleted: The authors declare that they have no conflict of interest.

Deleted: DRB and BMR were supported by the NASA CMS (NNX16AP33G) and the NSF Macrosystems Biology and NEON-Enabled Science (1926090) Programs

695 Bacour, C., Maignan, F., MacBean, N., Porcar-Castell, A., Flexas, J., Frankenberg, C., Peylin, P., Chevallier, F.,
696 Vuichard, N., and Bastrikov, V.: Improving Estimates of Gross Primary Productivity by Assimilating Solar-Induced
697 Fluorescence Satellite Retrievals in a Terrestrial Biosphere Model Using a Process-Based SIF Model, *J. Geophys.*
698 *Res. G: Biogeosci.*, 124, 3281–3306, <https://doi.org/10.1029/2019JG005040>, 2019.

699
700 Baldocchi, D. ‘Breathing’ of the terrestrial biosphere: lessons learned from a global network of carbon dioxide flux
701 measurement systems, *Aust. J. Bot.*, 56, 1–26, <https://doi.org/10.1071/BT07151>, 2008.

702
703 Baldocchi, D., Chu, H., and Reichstein, M.: Inter-annual variability of net and gross ecosystem carbon fluxes: A
704 review, *Agric. For. Meteorol.*, 249, 520–533, <https://doi.org/10.1016/j.agrformet.2017.05.015>, 2018.

705
706 [Bauerle, W. L., Oren, R., Way, D. A., Qian, S. S., Stoy, P. C., Thornton, P. E., Bowden, J. D., Hoffman, F. M., and
707 Reynolds, R. F.: Photoperiodic regulation of the seasonal pattern of photosynthetic capacity and the implications for
708 carbon cycling, *PNAS*, 109, 8612–8617, <https://doi.org/10.1073/pnas.1119131109>, 2012.](#)

709
710 Beer, C., Reichstein, M., Tomelleri, E., Ciais, P., Jung, M., Carvalhais, N., Rödenbeck, C., Arain, M. A., Baldocchi,
711 D., Bonan, G. B., Bondeau, A., Cescatti, A., Lasslop, G., Lindroth, A., Lomas, M., Luysaert, S., Margolis, H.,
712 Oleson, K. W., Rouspard, O., Veenendaal, E., Viovy, N., Williams, C., Woodward, F. I., and Papale, D.: Terrestrial
713 Gross Carbon Dioxide Uptake: Global Distribution and Covariation with Climate, *Science*, 329, 834–838,
714 <https://doi.org/10.1126/science.1184984>, 2010.

715
716 [Bergeron, O., Margolis, H. A., Black, T. A., Coursolle, C., Dunn, A. L., Barr, A. G., and Wofsy, S. C.: Comparison
717 of carbon dioxide fluxes over three boreal black spruce forests in Canada, *Global Change Biol.*, 13, 89–107,
718 <https://doi.org/10.1111/j.1365-2486.2006.01281.x>, 2007.](#)

719
720 Blanken, P.D., Monson, R.K., Burns, S.P., Bowling, D.R., Turnipseed, A.A.: Ameriflux US-NR1 Niwot Ridge
721 Forest (LTER NWT1), Ver. 16-5, AmeriFlux AMP, (Dataset). <https://doi.org/10.17190/AMF/1246088>, 2020.

722
723 Bloom, A. A. and Williams, M.: Constraining ecosystem carbon dynamics in a data-limited world: integrating
724 ecological “common sense” in a model–data fusion framework, *Biogeosciences*, 12, 1299–1315,
725 <https://doi.org/10.5194/bg-12-1299-2015>, 2015.

726
727 Bloom, A. A., Exbrayat, J.-F., Velde, I. R. van der, Feng, L., and Williams, M.: The decadal state of the terrestrial
728 carbon cycle: Global retrievals of terrestrial carbon allocation, pools, and residence times, *PNAS*, 113, 1285–1290,
729 <https://doi.org/10.1073/pnas.1515160113>, 2016.

730
731 [Bloom, A. A., Bowman, K. W., Liu, J., Konings, A. G., Worden, J. R., Parazoo, N. C., Meyer, V., Reager, J. T.,
732 Worden, H. M., Jiang, Z., Quetin, G. R., Smallman, T. L., Exbrayat, J.-F., Yin, Y., Saatchi, S. S., Williams, M., and
733 Schimel, D. S.: Lagged effects regulate the inter-annual variability of the tropical carbon balance, *Biogeosciences*,
734 17, 6393–6422, <https://doi.org/10.5194/bg-17-6393-2020>, 2020.](#)

735
736 [Bowling, D. R., Logan, B. A., Hufkens, K., Aubrecht, D. M., Richardson, A. D., Burns, S. P., Anderegg, W. R. L.,
737 Blanken, P. D., and Eiriksson, D. P.: Limitations to winter and spring photosynthesis of a Rocky Mountain
738 subalpine forest, *Agric. For. Meteorol.*, 252, 241–255, <https://doi.org/10.1016/j.agrformet.2018.01.025>, 2018.](#)

739
740 Buermann, W., Bikash, P. R., Jung, M., Burn, D. H., and Reichstein, M.: Earlier springs decrease peak summer
741 productivity in North American boreal forests, *Environ. Res. Lett.*, 8, 024027, <https://doi.org/10.1088/1748-9326/8/2/024027>, 2013.

742
743
744 Buermann, W., Forkel, M., O’Sullivan, M., Sitch, S., Friedlingstein, P., Haverd, V., Jain, A. K., Kato, E., Kautz, M.,
745 Lienert, S., Lombardozi, D., Nabel, J. E. M. S., Tian, H., Wiltshire, A. J., Zhu, D., Smith, W. K., and Richardson,
746 A. D.: Widespread seasonal compensation effects of spring warming on northern plant productivity, *Nature*, 562,
747 110–114, <https://doi.org/10.1038/s41586-018-0555-7>, 2018.

748

Deleted: Agricultural and Forest Meteorology

Deleted: ¶

Deleted: ¶

Deleted: Bloom, A. A., Bowman, K. W., Liu, J., Konings, A. G., Worden, J. R., Parazoo, N. C., Meyer, V., Reager, J. T., Worden, H. M., Jiang, Z., Quetin, G. R., Smallman, T. L., Exbrayat, J.-F., Yin, Y., Saatchi, S. S., Williams, M., and Schimel, D. S.: Lagged effects dominate the inter-annual variability of the 2010-2015 tropical carbon balance, 1–49, <https://doi.org/10.5194/bg-2019-459>, 2020. ¶

Deleted: Agricultural and Forest Meteorology

760 Burns, S. P., Blanken, P. D., Turnipseed, A. A., Hu, J., and Monson, R. K.: The influence of warm-season
761 precipitation on the diel cycle of the surface energy balance and carbon dioxide at a Colorado subalpine forest site,
762 *Biogeosciences*, 12, 7349–7377, <https://doi.org/10.5194/bg-12-7349-2015>, 2015
763
764 Chang, O., Xiao, X., Wu, X., Doughty, R., Jiao, W., Bajgain, R., Qin, Y., and Wang, J.: Estimating site-specific
765 optimum air temperature and assessing its effect on the photosynthesis of grasslands in mid- to high-latitudes,
766 *Environ. Res. Lett.*, 15, 034064, <https://doi.org/10.1088/1748-9326/ab70bb>, 2020.
767
768 Desai, A. R.: Climatic and phenological controls on coherent regional interannual variability of carbon dioxide flux
769 in a heterogeneous landscape, *J. Geophys. Res.: Biogeosci.*, 115, <https://doi.org/10.1029/2010JG001423>, 2010.
770
771 Ensinger, I., Sveshnikov, D., Campbell, D. A., Funk, C., Jansson, S., Lloyd, J., Shibistova, O., and Öquist, G.:
772 Intermittent low temperatures constrain spring recovery of photosynthesis in boreal Scots pine forests, *Global
773 Change Biol.*, 10, 995–1008, <https://doi.org/10.1111/j.1365-2486.2004.00781.x>, 2004.
774
775 Euskirchen, E. S., Carman, T. B., and McGuire, A. D.: Changes in the structure and function of northern Alaskan
776 ecosystems when considering variable leaf-out times across groupings of species in a dynamic vegetation model,
777 *Global Change Biol.*, 20, 963–978, <https://doi.org/10.1111/gcb.12392>, 2014.
778
779 Exbrayat, J.-F., Bloom, A. A., Falloon, P., Ito, A., Smallman, T. L., and Williams, M.: Reliability ensemble
780 averaging of 21st century projections of terrestrial net primary productivity reduces global and regional
781 uncertainties, *Earth Syst. Dynam.*, 9, 153–165, <https://doi.org/10.5194/esd-9-153-2018>, 2018.
782
783 Famiglietti, C. A., Smallman, T. L., Levine, P. A., Flack-Prain, S., Quetin, G. R., Meyer, V., Parazoo, N. C., Stettz,
784 S. G., Yang, Y., Bonal, D., Bloom, A. A., Williams, M., and Konings, A. G.: Optimal model complexity for
785 terrestrial carbon cycle prediction, *Biogeosciences*, 18, 2727–2754, <https://doi.org/10.5194/bg-18-2727-2021>, 2021.
786
787 Flynn, D. F. B. and Wolkovich, E. M.: Temperature and photoperiod drive spring phenology across all species in a
788 temperate forest community, *New Phytol.*, 219, 1353–1362, <https://doi.org/10.1111/nph.15232>, 2018.
789
790 Forkel, M., Carvalhais, N., Rödenbeck, C., Keeling, R., Heimann, M., Thonicke, K., Zaehle, S., and Reichstein, M.:
791 Enhanced seasonal CO₂ exchange caused by amplified plant productivity in northern ecosystems, *Science*, 351,
792 696–699, <https://doi.org/10.1126/science.aac4971>, 2016.
793
794 Fox, A., Williams, M., Richardson, A. D., Cameron, D., Gove, J. H., Quaife, T., Ricciuto, D., Reichstein, M.,
795 Tomelleri, E., Trudinger, C. M., and Van Wijk, M. T.: The REFLEX project: Comparing different algorithms and
796 implementations for the inversion of a terrestrial ecosystem model against eddy covariance data, *Agric. For.
797 Meteorol.*, 149, 1597–1615, <https://doi.org/10.1016/j.agrformet.2009.05.002>, 2009.
798
799 Frank, J. M., Massman, W. J., Ewers, B. E., Huckaby, L. S., and Negrón, J. F.: Ecosystem CO₂/H₂O fluxes are
800 explained by hydraulically limited gas exchange during tree mortality from spruce bark beetles, *J. Geophys. Res.*,
801 *Biogeosci.*, 119, 1195–1215, <https://doi.org/10.1002/2013JG002597>, 2014.
802
803 Goulden, M. and Bales, R.: California forest die-off linked to multi-year deep soil drying in 2012–2015 drought,
804 *Nat. Geosci.*, 12, 1, <https://doi.org/10.1038/s41561-019-0388-5>, 2019.
805
806 Greenland, D.: The Climate of Niwot Ridge, Front Range, Colorado, U.S.A., *Arct. Alp. Res.*, 21, 380–391,
807 <https://doi.org/10.1080/00040851.1989.12002751>, 1989.
808
809 Haario, H., Saksman, E., and Tamminen, J.: An Adaptive Metropolis Algorithm, *Bernoulli*, 7, 223–242,
810 <https://doi.org/10.2307/3318737>, 2001.
811
812 Hu, J., Moore, D. J. P., Burns, S. P., and Monson, R. K.: Longer growing seasons lead to less carbon sequestration
813 by a subalpine forest, *Global Change Biol.*, 16, 771–783, <https://doi.org/10.1111/j.1365-2486.2009.01967.x>, 2010.

Field Code Changed

Deleted: ¶

Deleted: Famiglietti, C. A., Smallman, T. L., Levine, P. A., Flack-Prain, S., Quetin, G. R., Meyer, V., Parazoo, N. C., Stettz, S. G., Yang, Y., Bonal, D., Bloom, A. A., Williams, M., and Konings, A. G.: Optimal model complexity for terrestrial carbon cycle prediction, *Biogeochemistry: Modelling, Terrestrial*, <https://doi.org/10.5194/bg-2020-478>, 2020.

Deleted: ¶

Deleted: ¶

Deleted: Nature Geoscience

Deleted: ¶
Goulden, M. L., Anderson, R. G., Bales, R. C., Kelly, A. E., Meadows, M., and Winston, G. C.: Evapotranspiration along an elevation gradient in California's Sierra Nevada, 117, <https://doi.org/10.1029/2012JG002027>, 2012. ¶

Deleted: Greenland, D.: The Climate of Niwot Ridge, Front Range, Colorado, U.S.A., 21, 380–391, <https://doi.org/10.1080/00040851.1989.12002751>, 1989. ¶
Haario, H., Saksman, E., and Tamminen, J.: An adaptive Metropolis algorithm, *Bernoulli*, 7, 223–242, 2001.

Deleted: ¶

838 Huxman, T. E., Turnipseed, A. A., Sparks, J. P., Harley, P. C., and Monson, R. K.: Temperature as a control over
839 ecosystem CO₂ fluxes in a high-elevation, subalpine forest, *Oecologia*, 134, 537–546,
840 <https://doi.org/10.1007/s00442-002-1131-1>, 2003.

841

842 Ishida, A., Nakano, T., Sekikawa, S., Maruta, E., and Masuzawa, T.: Diurnal changes in needle gas exchange in
843 alpine *Pinus pumila* during snow-melting and summer seasons, *Ecol. Res.*, 16, 107–116,
844 <https://doi.org/10.1046/j.1440-1703.2001.00376.x>, 2001.

845

846 Kattge, J. and Knorr, W.: Temperature acclimation in a biochemical model of photosynthesis: a reanalysis of data
847 from 36 species, *Plant Cell Environ.*, 30, 1176–1190, <https://doi.org/10.1111/j.1365-3040.2007.01690.x>, 2007.

848

849 Keenan, T. F., Davidson, E., Moffat, A. M., Munger, W., and Richardson, A. D.: Using model-data fusion to
850 interpret past trends, and quantify uncertainties in future projections, of terrestrial ecosystem carbon cycling, *Global*
851 *Change Biol.*, 18, 2555–2569, <https://doi.org/10.1111/j.1365-2486.2012.02684.x>, 2012.

852

853 Keenan, T. F., Gray, J., Friedl, M. A., Toomey, M., Bohrer, G., Hollinger, D. Y., Munger, J. W., O’Keefe, J.,
854 Schmid, H. P., Wing, I. S., Yang, B., and Richardson, A. D.: Net carbon uptake has increased through warming-
855 induced changes in temperate forest phenology, *Nat. Clim. Change*, 4, 598–604,
856 <https://doi.org/10.1038/nclimate2253>, 2014.

857

858 Knowles, J. F., Burns, S. P., Blanken, P. D., and Monson, R. K.: Fluxes of energy, water, and carbon dioxide from
859 mountain ecosystems at Niwot Ridge, Colorado, *Plant Ecol. Divers.*, 8, 663–676,
860 <https://doi.org/10.1080/17550874.2014.904950>, 2015.

861

862 Knowles, J. F., Molotch, N. P., Trujillo, E., and Litvak, M. E.: Snowmelt-Driven Trade-Offs Between Early and
863 Late Season Productivity Negatively Impact Forest Carbon Uptake During Drought, *Geophys. Res. Lett.*, 45, 3087–
864 3096, <https://doi.org/10.1002/2017GL076504>, 2018.

865

866 Korzukhin, M. D., Ter-Mikaelian, M. T., and Wagner, R. G.: Process versus empirical models: which approach for
867 forest ecosystem management?, *Can. J. For. Res.*, 26, <https://doi.org/10.1139/x26-096>, 2011.

868

869 Lasslop, G., Reichstein, M., Papale, D., Richardson, A. D., Arneeth, A., Barr, A., Stoy, P., and Wohlfahrt, G.:
870 Separation of net ecosystem exchange into assimilation and respiration using a light response curve approach:
871 critical issues and global evaluation, *Global Change Biol.*, 16, 187–208, [https://doi.org/10.1111/j.1365-](https://doi.org/10.1111/j.1365-2486.2009.02041.x)
872 [2486.2009.02041.x](https://doi.org/10.1111/j.1365-2486.2009.02041.x), 2009.

873

874 Lin, J. C., Mallia, D. V., Wu, D., and Stephens, B. B.: How can mountaintop CO₂ observations be used to constrain
875 regional carbon fluxes?, *Atmos. Chem. Phys.*, 17, 5561–5581, <https://doi.org/10.5194/acp-17-5561-2017>, 2017.

876

877 López-Blanco, E., Exbrayat, J.-F., Lund, M., Christensen, T. R., Tamstorf, M. P., Slevin, D., Hugelius, G., Bloom,
878 A. A., and Williams, M.: Evaluation of terrestrial pan-Arctic carbon cycling using a data-assimilation system, *Earth*
879 *Syst. Dynam.*, 10, 233–255, <https://doi.org/10.5194/esd-10-233-2019>, 2019.

880

881 Magney, T. S., Bowling, D. R., Logan, B. A., Grossmann, K., Stutz, J., Blanken, P. D., Burns, S. P., Cheng, R.,
882 Garcia, M. A., Köhler, P., Lopez, S., Parazoo, N. C., Raczka, B., Schimel, D., and Frankenberg, C.: Mechanistic
883 evidence for tracking the seasonality of photosynthesis with solar-induced fluorescence, *PNAS*, 116, 11640–11645,
884 <https://doi.org/10.1073/pnas.1900278116>, 2019.

885

886 Mayr, S., Schmid, P., Laur, J., Rosner, S., Charra-Vaskou, K., Dämon, B., and Hacke, U. G.: Uptake of Water via
887 Branches Helps Timberline Conifers Refill Embolized Xylem in Late Winter, *Plant Physiol.*, 164, 1731–1740,
888 <https://doi.org/10.1104/pp.114.236646>, 2014.

889

890 Medlyn, B. E., Dreyer, E., Ellsworth, D., Forstreuter, M., Harley, P. C., Kirschbaum, M. U. F., Roux, X. L.,
891 Montpied, P., Strassmeyer, J., Walcroft, A., Wang, K., and Loustau, D.: Temperature response of parameters of a
892 biochemically based model of photosynthesis. II. A review of experimental data, *Plant Cell Environ.*, 25, 1167–
893 [1179, <https://doi.org/10.1046/j.1365-3040.2002.00891.x>, 2002.](https://doi.org/10.1046/j.1365-3040.2002.00891.x)

Deleted: ¶

Deleted: ¶

Deleted: ¶

902
903 Monson, R. K., Turnipseed, A. A., Sparks, J. P., Harley, P. C., Scott-Denton, L. E., Sparks, K., and Huxman, T. E.:
904 Carbon sequestration in a high-elevation, subalpine forest, *Global Change Biol.*, 8, 459–478,
905 <https://doi.org/10.1046/j.1365-2486.2002.00480.x>, 2002.

906
907 Moore, D. J. P., Hu, J., Sacks, W. J., Schimel, D. S., and Monson, R. K.: Estimating transpiration and the sensitivity
908 of carbon uptake to water availability in a subalpine forest using a simple ecosystem process model informed by
909 measured net CO₂ and H₂O fluxes, *Agric. For. Meteorol.*, 148, 1467–1477,
910 <https://doi.org/10.1016/j.agrformet.2008.04.013>, 2008.

911
912 Myneni, R. B., Keeling, C. D., Tucker, C. J., Asrar, G., and Nemani, R. R.: Increased plant growth in the northern
913 high latitudes from 1981 to 1991, *Nature*, 386, 698–702, <https://doi.org/10.1038/386698a0>, 1997.

914
915 Öquist, G. and Huner, N. P. A.: Photosynthesis of Overwintering Evergreen Plants, *Annu. Rev. Plant Biol.*, 54, 329–
916 355, <https://doi.org/10.1146/annurev.arplant.54.072402.115741.2003>.

917
918 Parazoo, N. C., Arneeth, A., Pugh, T. A. M., Smith, B., Steiner, N., Luus, K., Commane, R., Benmergui, J.,
919 Stofferahn, E., Liu, J., Rödenbeck, C., Kawa, R., Euskirchen, E., Zona, D., Arndt, K., Oechel, W., and Miller, C.:
920 Spring photosynthetic onset and net CO₂ uptake in Alaska triggered by landscape thawing, *Global Change Biol.*, 24,
921 3416–3435, <https://doi.org/10.1111/gcb.14283>, 2018.

922
923 Parazoo, N. C., Magney, T., Norton, A., Raczka, B., Bacour, C., Maignan, F., Baker, I., Zhang, Y., Qiu, B., Shi, M.,
924 MacBean, N., Bowling, D. R., Burns, S. P., Blanken, P. D., Stutz, J., Grossmann, K., and Frankenberg, C.: Wide
925 discrepancies in the magnitude and direction of modeled solar-induced chlorophyll fluorescence in response to light
926 conditions, *Biogeosciences*, 17, 3733–3755, <https://doi.org/10.5194/bg-17-3733-2020>, 2020.

927
928 Pierrat, Z., Nehemy, M. F., Roy, A., Magney, T., Parazoo, N. C., Laroque, C., Pappas, C., Sonnentag, O.,
929 Grossmann, K., Bowling, D. R., Seibt, U., Ramirez, A., Johnson, B., Helgason, W., Barr, A., and Stutz, J.: Tower-
930 Based Remote Sensing Reveals Mechanisms Behind a Two-phased Spring Transition in a Mixed-Species Boreal
931 Forest, *J. Geophys. Res.: Biogeosci.*, 126, <https://doi.org/10.1029/2020JG006191>, 2021.

932
933 Quetin, G. R., Bloom, A. A., Bowman, K. W., and Konings, A. G.: Carbon Flux Variability From a Relatively
934 Simple Ecosystem Model With Assimilated Data Is Consistent With Terrestrial Biosphere Model Estimates, *J. Adv.*
935 *Model. Earth Syst.*, 12, <https://doi.org/10.1029/2019MS001889>, 2020.

936
937 Randerson, J. T., Field, C. B., Fung, I. Y., and Tans, P. P.: Increases in early season ecosystem uptake explain recent
938 changes in the seasonal cycle of atmospheric CO₂ at high northern latitudes, *Geophys. Res. Lett.*, 26, 2765–2768,
939 <https://doi.org/10.1029/1999GL900500>, 1999.

940
941 Raupach, M. R., Rayner, P. J., Barrett, D. J., DeFries, R. S., Heimann, M., Ojima, D. S., Quegan, S., and
942 Schimmlius, C. C.: Model–data synthesis in terrestrial carbon observation: methods, data requirements and data
943 uncertainty specifications, *Global Change Biol.*, 11, 378–397, <https://doi.org/10.1111/j.1365-2486.2005.00917.x>,
944 2005.

945
946 Reichstein, M., Falge, E., Baldocchi, D., Papale, D., Aubinet, M., Berbigier, P., Bernhofer, C., Buchmann, N.,
947 Gilmanov, T., Granier, A., Grünwald, T., Havránková, K., Ilvesniemi, H., Janous, D., Knohl, A., Laurila, T., Lohila,
948 A., Loustau, D., Matteucci, G., Meyers, T., Miglietta, F., Ourcival, J.-M., Pumpanen, J., Rambal, S., Rotenberg, E.,
949 Sanz, M., Tenhunen, J., Seufert, G., Vaccari, F., Vesala, T., Yakir, D., and Valentini, R.: On the separation of net
950 ecosystem exchange into assimilation and ecosystem respiration: review and improved algorithm, *Global Change*
951 *Biol.*, 11, 1424–1439, <https://doi.org/10.1111/j.1365-2486.2005.001002.x>, 2005.

952
953 Richardson, A. D., Williams, M., Hollinger, D. Y., Moore, D. J. P., Dail, D. B., Davidson, E. A., Scott, N. A.,
954 Evans, R. S., Hughes, H., Lee, J. T., Rodrigues, C., and Savage, K.: Estimating parameters of a forest ecosystem C
955 model with measurements of stocks and fluxes as joint constraints, *Oecologia*, 164, 25–40,
956 <https://doi.org/10.1007/s00442-010-1628-y>, 2010.

957

Deleted: cultural

Deleted: and

Deleted: est

Deleted: ogy

Deleted: ¶

Deleted: Parazoo, N. C., Magney, T., Norton, A., Raczka, B., Bacour, C., Maignan, F., Baker, I., Zhang, Y., Qiu, B., Shi, M., MacBean, N., Bowling, D. R., Burns, S. P., Blanken, P. D., Stutz, J., Grossman, K., and Frankenberg, C.: Wide Discrepancies in the Magnitude and Direction of Modelled SIF in Response to Light Conditions, 2020, 1–42, <https://doi.org/10.5194/bg-2019-508>, 2020.¶

Deleted: e2019MS001889,

971 Rowland, L., Hill, T. C., Stahl, C., Siebicke, L., Burban, B., Zaragoza-Castells, J., Ponton, S., Bonal, D., Meir, P.,
972 and Williams, M.: Evidence for strong seasonality in the carbon storage and carbon use efficiency of an Amazonian
973 forest, *Global Change Biol.*, 20, 979–991, <https://doi.org/10.1111/gcb.12375>, 2014.
974

975 Schimel, D., Schneider, F. D., and JPL Carbon and Ecosystem Participants: Flux towers in the sky: global ecology
976 from space, *New Phytol.*, 224, 570–584, <https://doi.org/10.1111/nph.15934>, 2019.
977

978 Scott-Denton, L. E., Moore, D. J. P., Rosenbloom, N. A., Kittel, T. G. F., Burns, S. P., Schimel, D. S., and Monson,
979 R. K.: Forecasting net ecosystem CO₂ exchange in a subalpine forest using model data assimilation combined with
980 simulated climate and weather generation, *J. Geophys. Res. G: Biogeosci.*, 118, 549–565,
981 <https://doi.org/10.1002/jgrg.20039>, 2013.
982

983 Sippel, S., Forkel, M., Rammig, A., Thonicke, K., Flach, M., Heimann, M., Otto, F. E. L., Reichstein, M., and
984 Mahecha, M. D.: Contrasting and interacting changes in simulated spring and summer carbon cycle extremes in
985 European ecosystems, *Environ. Res. Lett.*, 12, 075006, <https://doi.org/10.1088/1748-9326/aa7398>, 2017.
986

987 Smallman, T. L., Exbrayat, J.-F., Mencuccini, M., Bloom, A. A., and Williams, M.: Assimilation of repeated woody
988 biomass observations constrains decadal ecosystem carbon cycle uncertainty in aggrading forests, *J. Geophys. Res.*
989 *G: Biogeosci.*, 122, 528–545, <https://doi.org/10.1002/2016JG003520>, 2017.
990

991 Smith, W. K., Fox, A. M., MacBean, N., Moore, D. J. P., and Parazoo, N. C.: Constraining estimates of terrestrial
992 carbon uptake: new opportunities using long-term satellite observations and data assimilation, *New Phytol.*, 225,
993 105–112, <https://doi.org/10.1111/nph.16055>, 2020.
994

995 Stavros, E. N., Schimel, D., Pavlick, R., Serbin, S., Swann, A., Duncanson, L., Fisher, J. B., Fassnacht, F., Ustin, S.,
996 Dubayah, R., Schweiger, A., and Wennberg, P.: ISS observations offer insights into plant function, *Nat. Ecol. Evol.*,
997 1, 1–5, <https://doi.org/10.1038/s41559-017-0194>, 2017.
998

999 [Stinziano, J. R. and Way, D. A.: Autumn photosynthetic decline and growth cessation in seedlings of white spruce
1000 are decoupled under warming and photoperiod manipulations. *Plant Cell Environ.*, 40, 1296–1316,
1001 <https://doi.org/10.1111/pce.12917>, 2017.](https://doi.org/10.1111/pce.12917)
1002

1003 [Stinziano, J. R., Hüner, N. P. A., and Way, D. A.: Warming delays autumn declines in photosynthetic capacity in a
1004 boreal conifer, Norway spruce \(*Picea abies*\), *Tree Physiol.*, 35, 1303–1313, <https://doi.org/10.1093/treephys/tpv118>,
1005 2015.](https://doi.org/10.1093/treephys/tpv118)
1006

1007 Sun, Y., Frankenberg, C., Wood, J. D., Schimel, D. S., Jung, M., Guanter, L., Drewry, D. T., Verma, M., Porcar-
1008 Castell, A., Griffis, T. J., Gu, L., Magney, T. S., Köhler, P., Evans, B., and Yuen, K.: OCO-2 advances
1009 photosynthesis observation from space via solar-induced chlorophyll fluorescence, *Science*, 358,
1010 <https://doi.org/10.1126/science.aam5747>, 2017.
1011

1012 [Tanja, S., Berninger, F., Vesala, T., Markkanen, T., Hari, P., Mäkelä, A., Ilvesniemi, H., Hänninen, H., Nikinmaa,
1013 E., Huttula, T., Laurila, T., Aurela, M., Grelle, A., Lindroth, A., Arneth, A., Shibistova, O., and Lloyd, J.: Air
1014 temperature triggers the recovery of evergreen boreal forest photosynthesis in spring, *Global Change Biol.*, 9, 1410–
1015 1426, <https://doi.org/10.1046/j.1365-2486.2003.00597.x>, 2003.](https://doi.org/10.1046/j.1365-2486.2003.00597.x)
1016

1017 Thurner, M., Beer, C., Santoro, M., Carvalhais, N., Wutzler, T., Schepaschenko, D., Shvidenko, A., Kompter, E.,
1018 Ahrens, B., Levick, S. R., and Schimel, D. S.: Carbon stock and density of northern boreal and temperate forests,
1019 *Global Change Biol.*, 23, 297–310, <https://doi.org/10.1111/gcb.12125>, 2014.
1020

1021 Turnipseed, A. A., Blanken, P. D., Anderson, D. E., and Monson, R. K.: Energy budget above a high-elevation
1022 subalpine forest in complex topography, *Agric. For. Meteorol.*, 110, 177–201, [https://doi.org/10.1016/S0168-
1023 1923\(01\)00290-8](https://doi.org/10.1016/S0168-1923(01)00290-8), 2002.
1024

Deleted: ogist

Deleted: utural and

Deleted: Forest

Deleted: Meteorology

1029 Turnipseed, A. A., Anderson, D. E., Burns, S., Blanken, P. D., and Monson, R. K.: Airflows and turbulent flux
1030 measurements in mountainous terrain: Part 2: Mesoscale effects, *Agric. For. Meteorol.*, 125, 187–205,
1031 <https://doi.org/10.1016/j.agrformet.2004.04.007>, 2004.

1032 Wang, Y.-P., Trudinger, C. M., and Enting, I. G.: A review of applications of model–data fusion to studies of
1033 terrestrial carbon fluxes at different scales, *Agric. For. Meteorol.*, 149, 1829–1842,
1034 <https://doi.org/10.1016/j.agrformet.2009.07.009>, 2009.

1035 Williams, M., Rastetter, E. B., Fernandes, D. N., Goulden, M. L., Wofsy, S. C., Shaver, G. R., Melillo, J. M.,
1036 Munger, J. W., Fan, S.-M., and Nadelhoffer, K. J.: Modelling the soil–plant–atmosphere continuum in a Quercus–
1037 Acer stand at Harvard Forest: the regulation of stomatal conductance by light, nitrogen and soil/plant hydraulic
1038 properties, *Plant Cell Environ.*, 19, 911–927, <https://doi.org/10.1111/j.1365-3040.1996.tb00456.x>, 1996.

1039 Williams, M., Rastetter, E. B., Fernandes, D. N., Goulden, M. L., Shaver, G. R., and Johnson, L. C.: Predicting
1040 Gross Primary Productivity in Terrestrial Ecosystems, *Ecol. Appl.*, 7, 882–894, [https://doi.org/10.1890/1051-0761\(1997\)007\[0882:PGPPIT\]2.0.CO;2](https://doi.org/10.1890/1051-0761(1997)007[0882:PGPPIT]2.0.CO;2), 1997.

1041 Williams, M., Law, B. E., Anthoni, P. M., and Unsworth, M. H.: Use of a simulation model and ecosystem flux data
1042 to examine carbon–water interactions in ponderosa pine, *Tree Physiol.*, 21, 287–298,
1043 <https://doi.org/10.1093/treephys/21.5.287>, 2001.

1044 Williams, M., Schwarz, P. A., Law, B. E., Irvine, J., and Kurpius, M. R.: An improved analysis of forest carbon
1045 dynamics using data assimilation, *Global Change Biol.*, 11, 89–105, <https://doi.org/10.1111/j.1365-2486.2004.00891.x>, 2005.

1046 Williams, M. W., Seastedt, T. R., Bowman, W. D., McKnight, D. M., and Suding, K. N.: An overview of research
1047 from a high elevation landscape: the Niwot Ridge, Colorado Long Term Ecological Research programme, *Plant
1048 Ecol. Divers.*, 8, 597–605, <https://doi.org/10.1080/17550874.2015.1123320>, 2015.

1049 Winchell, T. S., Barnard, D. M., Monson, R. K., Burns, S. P., and Molotch, N. P.: Earlier snowmelt reduces
1050 atmospheric carbon uptake in midlatitude subalpine forests, *Geophys. Res. Lett.*, 43, 8160–8168,
1051 <https://doi.org/10.1002/2016GL069769>, 2016.

1052 [Wolf, S., Keenan, T. F., Fisher, J. B., Baldocchi, D. D., Desai, A. R., Richardson, A. D., Scott, R. L., Law, B. E.,
1053 Litvak, M. E., Brunsell, N. A., Peters, W., and van der Laan-Luijckx, I. T.: Warm spring reduced carbon cycle impact
1054 of the 2012 US summer drought, *PNAS*, 113, 5880, <https://doi.org/10.1073/pnas.1519620113>, 2016.](https://doi.org/10.1073/pnas.1519620113)

1055 Wutzler, T., Lucas-Moffat, A., Migliavacca, M., Knauer, J., Sickel, K., Šigut, L., Menzer, O., and Reichstein, M.:
1056 Basic and extensible post-processing of eddy covariance flux data with REddyProc, *Biogeosciences*, 15, 5015–5030,
1057 <https://doi.org/10.5194/bg-15-5015-2018>, 2018.

1058 Xu, C., Liu, H., Williams, A. P., Yin, Y., and Wu, X.: Trends toward an earlier peak of the growing season in
1059 Northern Hemisphere mid-latitudes, *Global Change Biol.*, 22, 2852–2860, <https://doi.org/10.1111/gcb.13224>, 2016.

1060 [Yang, Q., Blanco, N. E., Hermida-Carrera, C., Lehotai, N., Hurry, V., and Strand, Å.: Two dominant boreal conifers
1061 use contrasting mechanisms to reactivate photosynthesis in the spring, *Nat Commun.*, 11, 128,
1062 <https://doi.org/10.1038/s41467-019-13954-0>, 2020.](https://doi.org/10.1038/s41467-019-13954-0)

1063 Yin, Y., Bloom, A. A., Worden, J., Saatchi, S., Yang, Y., Williams, M., Liu, J., Jiang, Z., Worden, H., Bowman, K.,
1064 Frankenberg, C., and Schimel, D.: Fire decline in dry tropical ecosystems enhances decadal land carbon sink, *Nat
1065 Commun.*, 11, 1900, <https://doi.org/10.1038/s41467-020-15852-2>, 2020.

Deleted: ultural and

Deleted: Forest

Deleted: Meteorology

Deleted: Agricultural

Deleted: and

Deleted: est

Deleted: Meteorology

Deleted: Physiology

Deleted: ¶

Deleted: ¶

Deleted: ¶
Wolf, S., Keenan, T. F., Fisher, J. B., Baldocchi, D. D.,
Desai, A. R., Richardson, A. D., Scott, R. L., Law, B. E.,
Litvak, M. E., Brunsell, N. A., Peters, W., and van der Laan-
Luijckx, I. T.: Warm spring reduced carbon cycle impact of
the 2012 US summer drought, *Proc Natl Acad Sci USA*, 113,
5880, <https://doi.org/10.1073/pnas.1519620113>, 2016.¶

Deleted: ¶